RSC Advances

PAPER

View Article Online
View Journal | View Issue

Cite this: *RSC Adv.*, 2021, **11**, 37726

Co(II), Ni(II), Cu(II) and Cd(II)-thiocarbonohydrazone complexes: spectroscopic, DFT, thermal, and electrical conductivity studies†

R. Fouad, *[a] Ibrahim A. Shaaban,[bc] Tarik E. Ali,[ba] Mohammed A. Assiri[b] and S. S. Shenouda[d]

New and stable coordinated compounds have been isolated in a good yield. The chelates have been prepared by mixing Co(II), Ni(II), Cu(II), and Cd(II) metal ions with (1*E*)-1-((6-methyl-4-oxo-4*H*-chromen-3-yl)methylene)thiocarbonohydrazide (**MCMT**) in 2 : 1 stoichiometry (**MCMT** : M^{2+}). Various techniques, including elemental microanalyses, molar conductance, thermal studies, FT-IR, ^{1}H-NMR, UV-Vis, and XRD spectral analyses, magnetic moment measurements, and electrical conductivity, were applied for the structural and spectroscopic elucidation of the coordinating compounds. Further, computational studies using the DFT-B3LYP method were reported for **MCMT** and its metal complexes. **MCMT** behaves as a neutral NS bidentate moiety that forms octahedral complexes with general formula $[M(\mathbf{MCMT})_2Cl(OH_2)]Cl{\cdot}XH_2O$ ($M = Cu^{2+}$; ($X = \frac{1}{2}$), Ni^{2+}, Co^{2+}; ($X = 1$)); $[Cd(\mathbf{MCMT})_2Cl_2]{\cdot}\frac{1}{2}H_2O$. There is good confirmation between experimental infrared spectral data and theoretical DFT-B3LYP computational outcomes where **MCMT** acts as a five-membered chelate bonded to the metal ion through azomethine nitrogen and thiocarbonyl sulphur donors. The thermal analysis is studied to confirm the elucidated structure of the complexes. Also, the kinetic and thermodynamic parameters of the thermal decomposition steps were evaluated. The measured optical band gap values of the prepared compounds exhibited semiconducting nature. AC conductivity and dielectric properties of the ligand and its complexes were examined, which showed that Cu(II) complex has the highest dielectric constant referring to its high polarization and storage ability.

Received 14th September 2021
Accepted 27th October 2021

DOI: 10.1039/d1ra06902k

rsc.li/rsc-advances

1. Introduction

Thiocarbohydrazones dominate a large section of coordination chemistry owing to the flexibility of their structure, including several donor atoms for coordination with metals. The metal ion can successfully coordinate to thiocarbohydrazone through both its sulfur and nitrogen atoms, which is assumed to have medicinal activity in this class of compounds.[1–3] Also, both atoms allow the thiocarbohydrazone an opportunity to play an important role as chelating agents for forming stable complexes either in neutral or anionic form, usually acting as monodentate or bidentate ligands through S (thione) and N (azomethine) atoms.[4] Transition metal complexes with thiocarbohydrazone demonstrate pharmacological activity, inclusive of antifungal, antibacterial, antimalarial,[5–7] antitumor,[8,9] antiviral,[10] anti-cancer,[11] antioxidative,[12] antineoplastic,[13] antiproliferative,[14] and antitubercular[15] properties.

A wide range of research works was concerned with the biological properties of thiocarbohydrazone complexes, and limited works presented the semiconducting nature of these compounds. Hence significant attention has been devoted to examining the conductivity and electrical properties of these compounds.

Although the electrical conductivity of some transition metal complexes has been measured,[16,17] the electrical and dielectric properties of Co(II), Ni(II), Cu(II), and Cd(II)-(1*E*)-1-((6-methyl-4-oxo-4*H*-chromen-3-yl)methylene)thiocarbonohydraz-ide has not been reported yet.

Depending on the above facts, the present paper is devoted to the synthesis and spectroscopic characterization of thiocarbohydrazone and its Co(II), Ni(II), Cu(II), and Cd(II) complexes. Also, quantum mechanical (QM) calculations were carried out to verify the infrared spectral interpretation and resolve the preferred chelating site. AC electrical conductivity and dielectric properties of the prepared transition metal complexes were examined. The work was embraced to

[a]*Department of Chemistry, Faculty of Education, Ain Shams University, Roxy, Cairo, Egypt. E-mail: raniaahmed@edu.asu.edu.eg; Fax: +20 22581243; Tel: +201000212207*
[b]*Department of Chemistry, Faculty of Science, King Khalid University, P. O. Box 9004, Abha 61321, Saudi Arabia*
[c]*Department of Chemistry, Faculty of Science (Men's Campus), Al-Azhar University, Nasr City 11884, Cairo, Egypt*
[d]*Physics Department, Faculty of Education, Ain Shams University, Roxy, Cairo, Egypt*

† Electronic supplementary information (ESI) available. See DOI: 10.1039/d1ra06902k

demonstrate the likelihood for their uses in electronic applications through understanding their frequency response and providing information about their storage and dissipation of the electric fields.

2. Experimental details

2.1. Materials and characterization

The starting materials were analytical grade. Thiocarbohydrazide and 3-formylchromone are prepared according to the published literature.[18,19] The metal salts Co(II), Ni(II), Cu(II), and Cd(II) were used as chloride salts from BDH or Merck. Organic solvents were spectroscopic grade and were used as received.

Carbon, hydrogen, nitrogen, and sulfur microanalyses were conducted at the National Research Center in Dokki, Giza, Egypt. Complexometrically, the metal percentage in the complexes was estimated. A melting point apparatus (Stuart), England, was applied for detecting the melting or decomposition points. 10^{-3} M solutions of solid complexes in DMF were prepared for molar conductivity calculation by the corning conductivity meter NY 14831 model. A Shimadzu thermogravimetric analyzer was used to investigate TGA-DTG measurements from room temperature up to 800 °C. Using the FT-IR Nicolet IS10 spectrometer, FT-IR spectra (4000–400 cm^{-1}) of metal complexes were obtained. ^{1}H-NMR spectra were determined at room temperature on a 'Varian FT-290.90 MHZ' spectrometer. Dimethyl sulfoxide and DMSO-d_6, were used as the solvent and tetramethylsilane (TMS) as an internal reference. The UV-Vis (JASCO type V-550) spectrophotometer was used to measure the diffused reflectance of powder samples and to record electronic spectra of 10^{-3} M solid complexes, and DMF is used as a solvent. The Gouy system calculated the magnetic susceptibility of complexes at room temperature using Shelwood scientific, Cambridge Science Park, magnetic susceptibility balance (England). The effective magnetic moments were evaluated using the $\mu_{eff} = 2.828\ (X_m T)^{1/2}$ B.M. relationship, where X_m is the molar susceptibility corrected for the diamagnetism of all atoms in compounds using Pascal's constants. ESR spectra were recorded on the Bruker, Model: EMX, X-band spectrometer. PHILIPS diffractometer with CuKα_1 radiation ($k = 1.54056$ Å) was used to record the XRD patterns. A 40 kV accelerating voltage and a 30 mA emission current were applied. Resistance of the samples has been measured by Keithly electrometer (E-616A). The impedance, loss tangent and the capacitance of the samples have been measured using computerized PM-6304 Fluke & Phillips RCL Bridge.

2.2. Synthesis of (1*E*)-1-((6-methyl-4-oxo-4*H*-chromen-3-yl) methylene) thiocarbonohydrazide ligand (MCMT)

(1*E*)-1-((6-Methyl-4-oxo-4*H*-chromen-3-yl)methylene) thiocarbonohydrazide ligand (**MCMT**) was synthesized according to reported method.[20] Yield: 88%; mp ~193 °C; anal. found (calcd) for $C_{12}H_{12}N_4O_2S$: M_w (g): (276.31); % C: 52.22 (52.16); % H: 4.52 (4.37); % N: 20.30 (20.27); % S: 11.40 (11.60); FT-IR (KBr, ν, cm^{-1}): 3292, 3172 (NH_2,NH), 3057 $(CH)_{arom}$,1617 $(C{=}O)_{\gamma\text{-pyrone}}$, 1596 (CH=N), 1235, 815 (NH–C=S); ^{1}H-NMR (δ, ppm): 2.19 (s, 3H, CH_3), 4.19 (s, 2H, NH_2), 6.78–6.89 (m, 1H, H-8), 7.68–7.71 (m, 1H, H-7), 8.31 (s, 1H, H-5), 8.53 (s, 1H, CH=N), 9.14 (s, 1H, H-2), 10.41 (s, 1H, NH), 12.09 (s, 1H, NH). ^{13}C-NMR: 21.6 (CH_3), 116.8 (C-3), 118.0 (C-8), 125.7 (C-4a), 126.3 (C-5), 127.3 (C-6), 135.2 (C-7), 148.6 (C=N), 151.3 (C-8a), 154.2 (C-2), 174.1 (C=O), 185.0 (C=S); UV/Vis (DMF) λ_{max} (nm): 270, 296, 316, 345 and 410.

2.3. General method for the synthesis of transition metal complexes $[M(MCMT)_2OH_2Cl]Cl{\cdot}XH_2O$ ($M = Cu^{2+}$; ($X = \frac{1}{2}$), Ni^{2+}, Co^{2+}; ($X = 1$) and $[Cd(MCMT)_2Cl_2]{\cdot}\frac{1}{2}H_2O$

An ethanolic solution of **MCMT** (1.6 g, 6 mmol) was added to metal salts (3 mmol) namely, $CuCl_2{\cdot}6H_2O$, $NiCl_2{\cdot}6H_2O$, $CoCl_2{\cdot}6H_2O$, and $CdCl_2{\cdot}6H_2O$. The reaction mixture was refluxed for 8 h. The precipitate was filtered and washed several times with 50% (v/v) ethanol–water to remove any traces of unreacted starting materials. Finally, the precipitate was dried in vacuum desiccators over anhydrous $CaCl_2$ overnight. The dried complexes are $[Co(\mathbf{MCMT})_2(Cl)(H_2O)]Cl{\cdot}H_2O$; yield: 73%; mp > 300 °C; anal. found (calcd) for $C_{24}H_{28}N_8O_6S_2Cl_2Co$: M_w (g): (718.50); % C: 40.21 (40.11); % H: 3.75 (3.92); % N: 15.37 (15.59); % S: 8.69 (8.92); % Co: 8.11 (8.20); FT-IR (KBr, ν, cm^{-1}): 3432 (OH), 3168 (NH_2, NH), 3024 $(CH)_{arom}$, 1617 $(C{=}O)_{\gamma\text{-pyrone}}$, 1545 (CH=N), 1212, 788 (NH–C=S), 544 (M–O), 475 (M–N). Molar conductance (Λ_m): 85 ohm^{-1} mol^{-1} cm^2; UV/Vis (DMF) λ_{max} (nm): 288, 354, 399, 434, 660. μ_{eff} (B.M.): 4.4.

$[Ni(\mathbf{MCMT})_2(Cl)(H_2O)]Cl{\cdot}H_2O$; yield: 70%; mp > 300 °C; anal. found (calcd) for $C_{24}H_{28}N_8O_6S_2Cl_2Ni$: M_w (g): (718.26); % C: 40.31 (40.13); % H: 3.79 (3.92); % N: 15.38 (15.59); % S: 8.77 (8.92); % Ni: 8.09 (8.17); FT-IR (KBr, ν, cm^{-1}): 3424 (OH), 3166 (NH_2, NH), 3026 $(CH)_{arom}$, 1617 $(C{=}O)_{\gamma\text{-pyrone}}$, 1540 (CH=N), 1210, 790 (NHC=S), 544 (M–O), 478 (M–N). Molar conductance (Λ_m): 89 ohm^{-1} mol^{-1} cm^2; UV/Vis (DMF) λ_{max} (nm): 272, 354, 396, 451, 585; μ_{eff} (B.M.): 2.8.

$[Cu(\mathbf{MCMT})_2(Cl)(H_2O)]Cl{\cdot}\frac{1}{2}H_2O$; yield: 75%; mp > 300 °C; anal. found (calcd) for $C_{24}H_{27}N_8O_{5.5}S_2Cl_2Cu$: M_w (g): (714.10); % C: 40.54 (40.36); % H: 3.77 (3.81); % N: 15.55 (15.69); % S: 8.75 (8.98); % Cu: 8.67 (8.89); FT-IR (KBr, ν, cm^{-1}): 3426 (OH), 3193, 3170 (NH_2, NH), 3025 $(CH)_{arom}$, 1617 $(C{=}O)_{\gamma\text{-pyrone}}$, 1547 (CH=N), 1204, 789 (NH–C=S), 545 (M–O), 470 (M–N). Molar conductance (Λ_m): 90 ohm^{-1} mol^{-1} cm^2; UV/Vis (DMF) λ_{max} (nm): 274, 351, 394, 442, 580; μ_{eff} (B.M.):1.8. EPR (at room temperature, X-band): $g_{||} = 2.13$ and $g_{|} = 2.06$.

$[Cd(\mathbf{MCMT})_2(Cl)_2]{\cdot}\frac{1}{2}H_2O$; yield: 75%; mp > 300 °C; anal. found (calcd) for $C_{24}H_{25}N_8O_{4.5}S_2Cl_2Cd$: M_w (g): (744.96); % C: 38.49 (38.69); % H: 3.47 (3.38); % N: 15.10 (15.04); % S: 8.51 (8.60); % Cd: 15.30 (15.08); FT-IR (KBr, ν, cm^{-1}): 3440 (OH), 3178 (NH_2, NH), 3030 $(CH)_{arom}$, 1619 $(C{=}O)_{\gamma\text{-pyrone}}$, 1540 (CH=N), 1209, 793 (NH–C=S), 477 (M–N). (^{1}H-NMR, δ, ppm): 2.36 (s, 3H, CH_3), 3.88 (s, 2H, NH_2), 6.77–6.81 (m, 1H, H-8), 6.88–6.91 (m, 1H, H-8), 7.62–7.67 (m, 2H, H-7), 8.23 (s, 1H, H-5), 8.24 (s, 1H, H-5), 8.83 (s, 1H, CH=N), 8.84 (s, 1H, CH=N), 9.14 (s, 1H, H-2), 9.15 (s, 1H, H-2), 10.49 (br, 2H, CS<u>NH</u>NH_2), 12.19 (s, 2H, CH]N<u>NH</u>CS). Molar conductance (Λ_m): 15 ohm^{-1} mol^{-1} cm^2; UV/Vis (DMF) λ_{max} (nm): 288, 318, 417.

The chemical structures of the obtained metal complexes are represented in Scheme 1.

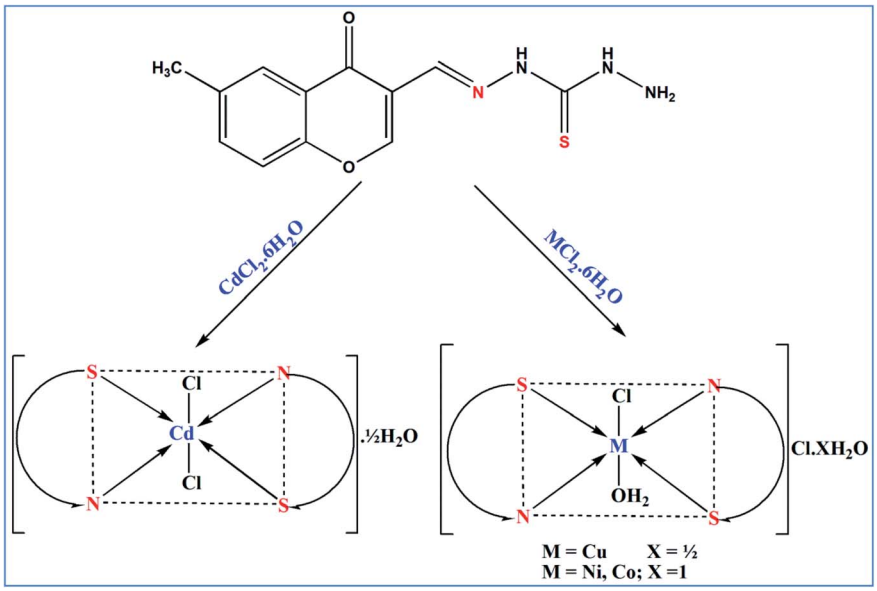

Scheme 1 Synthesis of transition metal complexes.

2.4. Computational methods

QM calculations in this work were performed based on density functional theory (DFT) using a B3LYP level,[21,22] which is a well-established method and broadly applied for transition metal complexes.[23–26] Standard 6-31G(d) basis set was used for all atoms except for the heavy Cd(II) ion where the effective core potential (ECP) LanL2DZ basis set was used[27] where the pseudo-potential of core electrons were included. Moreover, spin multiplicities of quartet, triplet, doublet, and singlet were used for Co(II), Ni(II), Cu(II), and Cd(II) complexes, respectively. All QM calculations reported herein were carried out employing the Gaussian 09 program package.[28] Based on the gradient method of Pulay,[29] full geometry optimization was achieved through simultaneous relaxation of all geometrical parameters until the convergence criteria of Gaussian 09 package was reached.[28] Subsequently, the vibrational frequencies were calculated to verify that the obtained optimized geometry belongs to true energy minima, which is indicated by the absence of imaginary frequencies. The *x*,*y*,*z* coordinates for all calculated structures along with their energies in atomic unit are provided in the ESI.†

3. Results and discussion

3.1. Physicochemical study

The performed synthesis involving the reaction of **MCMT** with metal chlorides in reflux system afforded, generally in good yield, four colorful complexes of empirical formula, $[M(\mathbf{MCMT})_2Cl(H_2O)]Cl\cdot XH_2O$; ($M = Cu^{2+}$; $X = \frac{1}{2}$; Ni^{2+}, Co^{2+}; $X = 1$) and $[Cd(\mathbf{MCMT})_2(Cl)_2]\cdot\frac{1}{2}H_2O$. These discrete complexes are quite stable in the air and can be maintained in a desiccator for a long time without any observed decomposition. All prepared complexes are soluble in Lewis bases such as DMF and DMSO but sparingly soluble in methanol and ethanol. The elemental analysis supports the suggested chemical structures of the complexes. As shown in Scheme 1, the complexes are formed in 1 : 2 metal-to-ligand stoichiometry. Moreover, the analytical data of metal chelates showed that the ligand behaves as a neutral bidentate.

The molar conductance values of ~1 mM solution for all prepared complexes were measured at room temperature in DMF. The molar conductance values for Co(II), Ni(II), and Cu(II) complexes are within the characteristic range of 1 : 1 electrolytes, indicating that one anion is located out of the coordination sphere as a counter ion.[30,31] On the other hand, the

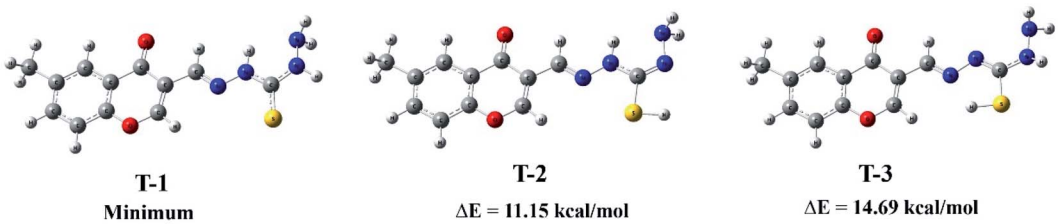

Fig. 1 Equilibrium geometries of suggested tautomers for MCMT and their relative energies (Δ*E*) using B3LYP/6-31G(d) calculations.

dissolved Cd(II) complex was characterized by non-electrolytic nature.[32,33]

3.2. Geometry structural study

After several recrystallization trials, we could not get the single crystals for the prepared metal complexes. Therefore, we took advantage of QM calculations to theoretically confirm the proposed structures for metal complexes. DFT-B3LYP calculations have been carried out to infer the preferred coordination sites of the ligand to the metal ion and to conclude the favored geometrical isomerism. The global reactivity descriptors and the order of coordination stability for the prepared metal complexes were also predicted.

Initially, we have dealt with the geometry of the **MCMT** ligand by exploring its tautomeric stability owing to intramolecular proton transfer from *imino* to *thiocarbonyl* group. Thus, three tautomeric structures were hypothetically proposed, *diamino-thione* (**T-1**) and two *imino-thiol* (**T-2** and **T-3**). Fig. 1 shows their fully optimized geometries obtained from B3LYP/6-31G(d) calculation along with their relative energies. Accordingly, the *diamino-thione* (**T-1**) was identified as the most stable tautomeric structure with the lowest energy and real vibrational frequencies. The *imino-thiol* tautomers, **T-2** and **T-3**, are higher in energy than **T-1** by 11.15 and 14.69 kcal mol^{-1}, respectively. These results agree with the experimental infrared spectrum of the ligand, where the characteristic band due to the S–H stretch vibration in the 2600–2400 cm^{-1} range was absent (Section 3.3.1). Employing B3LYP/6-31G(d) calculations, we have predicted the electrostatic potential (ESP) charges[34,35] to obtain the charge distributions for the most stable tautomer (**T-1**). The calculated ESP charges for **T-1** are given in the ESI, Fig. S1.† The computed ESP charges show a negative atomic charge for carbonyl O (−0.52), N_{az} (−0.45), thiocarbonyl S (−0.34), and amino N (−0.66). These values reflect the electron donating character of these atoms and can be coordinated to metal ions, *i.e.*, active coordination centers.

Owing to the presence of several active coordination centers in the ligand, five structures (**S-1** to **S-5**) were proposed with different possibilities for chelation of the ligand to the metal ion. Firstly, the ligand can form five-membered chelates through N_{az} and S (**S-1**), *imino* N (**S-2**), or *amino* N (**S-3**) donors. In addition, the five-membered chelation can occur *via* the bidentate coordination sites of *amino* and *imino* Ns (**S-4**). The fifth structure results from coordination through N_{az} and chromone carbonyl O (**S-5**), forming a six-membered chelate. Consequently, geometry optimization has been performed for these proposed structures (**S-1** to **S-5**) using Cu^{2+} as the metal ion. The equilibrium geometries for **S-1** to **S-5** as predicted using B3LYP/6-31G(d) calculations are shown in Fig. 2. The computational results favor **S-1** with minimum energy in agreement with the infrared spectral interpretation (Section 3.3.1). For structures **S-2** to **S-5**, high energy differences of 12.78–41.62 kcal mol^{-1} were predicted relative to **S-1**.

In view of these proposed structures of the complexes, five geometrical isomers could be suggested owing to the *cis* and *trans* orientations for each pair of coordination sites. The pair of N_{az}'s, S's, and Cl/H_2O coordination sites can be located *trans* to each other (**Isomer 1**, *all trans*) or in *cis* configuration (**Isomer 2**, *all cis*). For **Isomer 3**, N_{az}'s and S's were *cis* to each other while Cl/H_2O pair arranged in the *trans* orientation. The rearrangement of N_{az}'s/S's pairs to be *cis*/*trans* to each other and *vice versa* results in **Isomer 4** (*cis*-N_{az}'s and *trans*-S's) and **Isomer 5** (*trans*-N_{az}'s and *cis*-S's). The geometries of **Isomers 1–5** were fully optimized using B3LYP/6-31G(d) calculations for all complexes except Cd-ion, where the ECP-LanL2DZ basis set was used. Table 1 lists the computed energy along with the energy differences (ΔE) with respect to the most stable isomer for the investigated metal complexes. Also, the optimized geometries of geometrical isomers of Co(II), Ni(II), and Cu(II) complexes are displayed in Fig. 3. For the [Cd(**MCMT**)$_2$Cl$_2$] complex, the equilibrium geometries for its geometrical isomers are given in the ESI (Fig. S2†). As seen from the data in Table 1, **Isomer 1** (*all trans*) for the metal complexes under investigation was found to

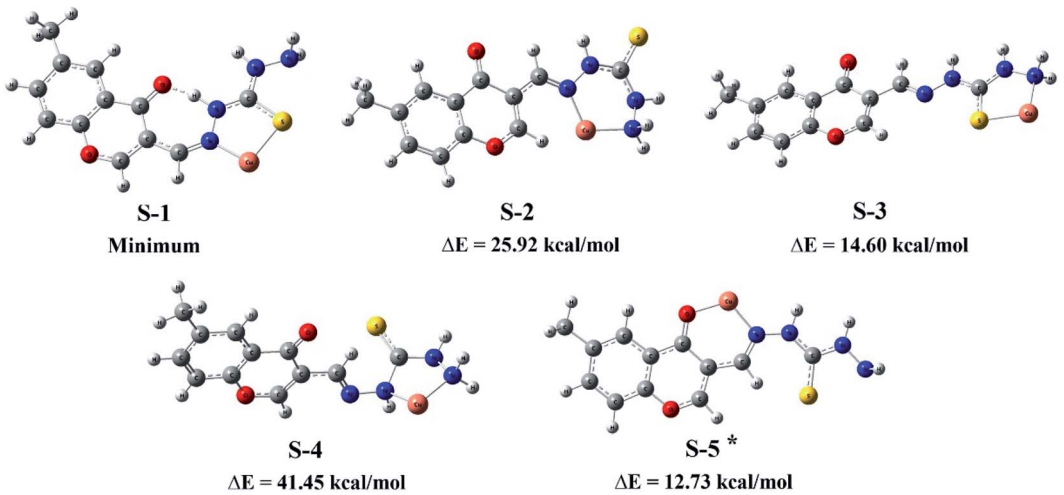

Fig. 2 Optimized geometries and relative energy for the proposed coordination sites for the ligand to Cu(II) ion. * **S-5** has an imaginary frequency (*i.e.*, transition state).

Table 1 DFT-B3LYP calculated energy (E, Hartree) and relative energy (ΔE, kcal mol^{-1}) for suggested geometrical isomer of the prepared metal complexes[a,b]

	Isomer 1[c]		Isomer 2[c]		Isomer 3[c]		Isomer 4[c]		Isomer 5[c]	
Complex	E	ΔE	E	ΔE	E	ΔE	E	ΔE	E	ΔE
Cu(II) complex	−4640.974656	0.0	−4640.919524	34.60	−4640.92091	33.73	−4640.921366	33.44	−4640.893092	51.18
Ni(II) complex	−4508.863215	0.0	−4508.829768	20.99	−4508.83659	16.71	−4508.831065	20.17	−4508.805617	36.14
Co(II) complex	−4383.342023	0.0	−4383.309348	20.50	−4383.30149	25.43	−4383.298181	27.51	−4383.294179	30.02
Cd(II) complex	−3432.53667	0.0	−3432.454744	51.41	−3432.33548	126.25	−3432.350125	117.06	−3432.353494	114.94

[a] Calculations were performed using 6-31G(d) basis set for all atoms except for Cd(II) ion where ECP-LanL2DZ basis set was used. [b] Energy differences (ΔE) are relative to the most stable **Isomer 1** (minimum energy). [c] For the structures of **Isomers 1–5**, see Fig. 3 (Co, Ni, and Cu-complexes) and Fig. S2 (Cd-complex).

be the most stable isomer with the lowest energy and real frequencies. These results were consistent with the reported crystal structure for Diaqua-bis(1,1-dimethylthiocarbazide) nickel(II) fumarate.[36] **Isomers 2–5** were disfavored with an energy difference of 16.71–126.25 kcal mol^{-1} compared to **Isomer 1**, which could account for the strain and the repulsion between the *cis*-oriented coordination site pairs.

The stability of the prepared metal complexes has been anticipated by calculating the binding energy between the metal ion and ligand and the coordination energy[37,38] as follows:

$$\Delta E = (E_{M^{2+}} + 2E_L + E_{Cl^-} + E_{H_2O}) - E_{[ML_2Cl(H_2O)]^+},\ M^{2+} = Co^{2+}, Ni^{2+} \text{ and } Cu^{2+}$$

$$\Delta E = (E_{M^{2+}} + 2E_L + 2E_{Cl^-}) - E_{[ML_2Cl_2]},\ M^{2+} = Cd^{2+}$$

where $E_{M^{2+}}$, E_L, E_{Cl^-}, E_{H_2O}, $E_{[ML_2Cl(H_2O)]^+}$ and $E_{[ML_2Cl_2]}$ are the computed energies using DFT-B3LYP calculations at 6-31G(d) basis set for all atoms excluding Cd atom, where LanL2DZ basis set was used. The computational results predict coordination energies of 442.24, 544.34, 581.35, and 583.02 kcal mol^{-1} for Cd(II), Co(II), Ni(II), and Cu(II) complexes, respectively. The positive values for coordination energy infer the highly stable form of the investigated metal complexes. Additionally, the coordination stabilities were in the order of Cu(II) ← N > Ni(II) ← N > Co(II) ← N, which agrees with the relative stabilities of complexes formed by the first row divalent metal ions reported by the Irving–Williams series.[39]

Energies for the frontier highest occupied/lowest unoccupied molecular orbitals; (HOMO/LUMO) have been computed for **MCMT** (**S-1**) and their metal complexes in the most stable isomer (1, *all trans*). Afterwards, a set of electronic properties (see Table 2) describing molecular reactivity/stability such as, energy gap (E_g), chemical potential (μ), hardness (η), electronegativity (χ), and electrophilicity index (ω) were predicted.[40,41] The HOMO's and LUMO's of the **MCMT** ligand and its Co(II) complex are displayed in Fig. 4. For **MCMT**, the HOMO was mainly delocalized over the thiocarbonyl group along with azomethine N with a low extent, which refers to strong electron donation of those moieties. Therefore, **MCMT** was preferred to chelate metal ions *via* these moieties. The HOMO of Co(II) complex has a large contribution from Cl, C=S, and H_2O coordinated ligands. However, the LUMO of **MCMT** and Co(II)

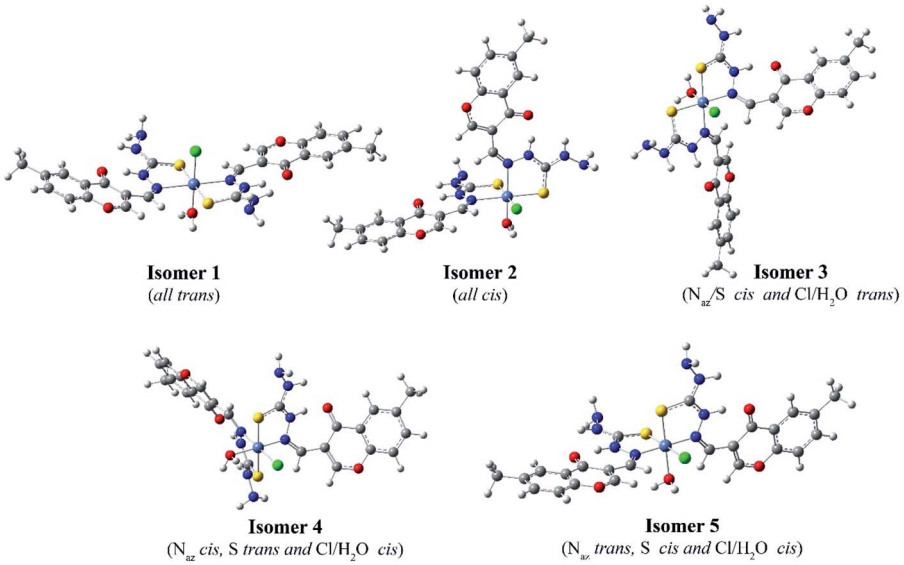

Fig. 3 DFT-B3LYP/6-31G(d) optimized geometries of the suggested geometrical isomers for Co(II), Ni(II), and Cu(II) complexes.

Table 2 Calculated molecular reactivity descriptors for ligand and its metal complexes[a]

Molecular parameters	Ligand	Cu-complex	Ni-complex	Co-complex	Cd-complex
E(HOMO) a.u.	−0.19788	−0.25513	−0.24876	−0.24568	−0.13939
E(HOMO) eV	−5.385	−6.942	−6.769	−6.685	−3.793
E(LUMO) a.u.	−0.06025	−0.15521	−0.15734	−0.15725	−0.07795
E(LUMO) eV	−1.639	−4.224	−4.281	−4.279	−2.121
ΔE(LUMO–HOMO) eV	3.745	2.719	2.488	2.406	1.672
Ionization potential, IP eV	5.385	6.942	6.769	6.685	3.793
Electron affinity, EA eV	1.639	4.224	4.281	4.279	2.121
Electronegativity, χ eV	3.512	5.583	5.525	5.482	2.957
Chemical potential, μ eV	−3.512	−5.583	−5.525	−5.482	−2.957
Chemical hardness, η eV	1.873	1.359	1.244	1.203	0.836
Chemical softness, s eV	0.267	0.368	0.402	0.416	0.598
Global electrophilicity index, ω eV	3.294	11.464	12.272	12.490	5.230
Total dipole moment, μ_{tot} debye	3.623	2.252	3.239	3.102	1.747

[a] Calculations were performed using B3LYP method and 6-31G(d) basis set for all atoms except for Cd(II) ion where ECP-LanL2DZ basis set was used. For metal complexes, calculations were performed for the most stable **Isomer 1** (minimum energy).

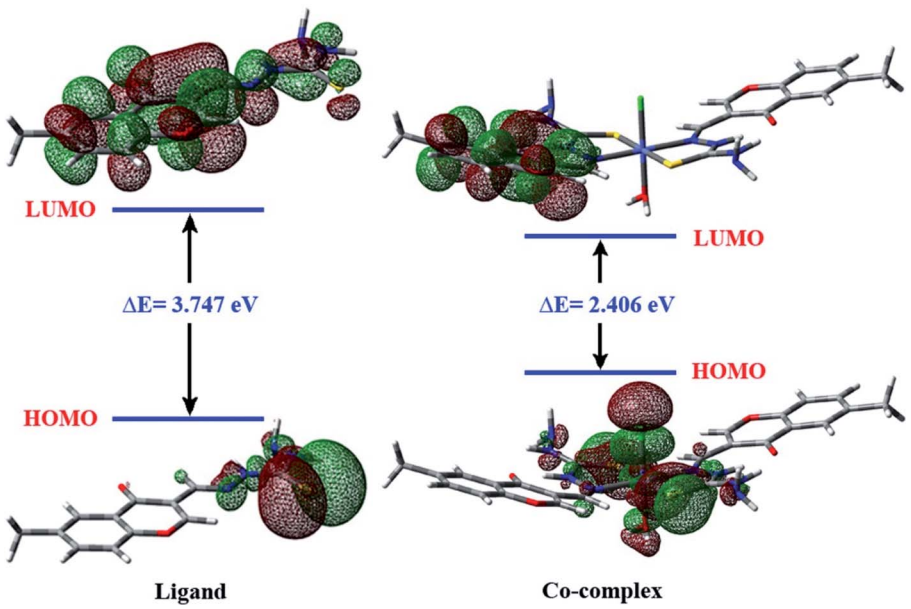

Fig. 4 HOMO and LUMO frontier molecular orbitals for MCMT ligand and its Co(II) complex as predicted using B3LYP/6-31G(d) calculations.

complex was found to be distributed over one chromone moiety.

The HOMO–LUMO energy gap (E_g) is a useful metric for predicting molecular stability and chemical reactivity, along with biological activity. Molecules with a small energy gap are anticipated to have a high chemical reactivity[42] and result in a significant degree of intramolecular charge transfer reactions, which affect and elevate the bioactivity.[43,44] In this work, the investigated metal complexes exhibit low values of energy gap (1.672–2.719 eV, see Table 2), implying that they are biologically potent. In addition, the predicted negative values of chemical potential indicate the stability of the complexes, *i.e.*, they do not spontaneously decompose. As shown in Table 2, the Co(II) complex exhibits the highest value of electrophilicity (ω) and reveals a high ability to accept electrons.

3.3. Thermal study

The TGA analysis of synthesized complexes offers valuable details on the stability of the complexes. The steps of thermal degradation of transition metal complexes are presented in Table 3.

A good consensus exists between thermal and analytical data suggested by the theoretical formula. The Co(II), Ni(II), Cu(II), and Cd(II) complexes lose lattice water molecules and become anhydrous at 110, 109, 94, and 106 °C, respectively. There are two routes to remove the coordinated water. In the first route, the coordinated water was removed separately as in Ni(II) and Co(II) complexes at 150 and 160 °C, respectively.

In the second route, coordinated water molecule removal was followed by releasing Cl_2 molecule as in the Cu(II) complex at 239 °C. For Ni(II) and Cd(II) complexes, the Cl_2 molecule was

Table 3 Thermal analysis of thiocarbohydrazone complexes

Compound	Temp range °C	% Total loss in weight found (calc.)	Composition of the residue	Probable composition of the expelled groups
Co(II) complex	30.0–110	2.45 (2.51)	$C_{24}H_{26}N_8O_5S_2Cl_2Co$	One molecule of lattice H_2O
	110–160	5.00 (5.02)	$C_{24}H_{24}N_8O_4S_2Cl_2Co$	One molecule of coordinated H_2O
	161–385	32.0 (31.9)	$C_{22}H_{16}N_4O_4S_2Co$	Two molecules of Cl_2, NH_3 and HCN
	386–566	48.5 (48.4)	$C_{20}H_{14}N_2O_4Co$	Two molecules of HSCN
Ni(II) complex	30.0–109	2.50 (2.50)	$C_{24}H_{26}N_8O_5S_2Cl_2Ni$	One molecule of lattice H_2O
	110–150	4.80 (5.00)	$C_{24}H_{24}N_8O_4S_2Cl_2Ni$	One molecule of coordinated water
	151–253	15.0 (14.8)	$C_{24}H_{24}N_8O_4S_2Ni$	One molecule of Cl_2
	254–364	31.5 (31.8)	$C_{22}H_{16}N_4O_4S_2Ni$	Two molecules of NH_3 and HCN
	365–522	48.5 (48.3)	$C_{20}H_{14}N_2O_4Ni$	Two molecules of HSCN
Cu(II) complex	30.0–94	3.25 (1.26)	$C_{24}H_{26}N_8S_2O_5Cl_2Cu$	Half molecule of lattice H_2O
	95.0–239	24.0 (13.7)	$C_{24}H_{24}N_8S_2O_4Cu$	One molecule of coordinated H_2O and one molecule of Cl_2.
	240–437	47.5 (47.3)	$C_{20}H_{14}N_2O_4Cu$	Two molecules of NH_3, HCN and HSCN
Cd(II) complex	30.0–106	1.10 (1.20)	$C_{24}H_{24}N_8O_4S_2Cl_2Cd$	Half molecule of lattice H_2O
	107–232	10.9 (10.7)	$C_{24}H_{24}N_8O_4S_2Cd$	One molecule of Cl_2.
	233–269	20.0 (19.8)	$C_{24}H_{18}N_6O_4S_2Cd$	Two molecules of NH_3.
	270–306	27.0 (27.1)	$C_{22}H_{16}N_4O_4S_2Cd$	Two molecules of HCN
	307–479	43.0 (42.9)	$C_{20}H_{14}N_2O_4Cd$	Two molecules of HSCN

removed separately at 253 and 232 °C, respectively. On the other hand, the removal of Cl_2 molecule was eliminated with a partial decomposition of the ligand at 385 °C as in Co(II) complex.

The Cu(II) complex continues its decomposition within the temperature range of 240–437 °C with a weight loss of 47.3% assignable to the removal of two molecules of NH_3, HCN, and HSCN.

For Ni(II) complex, the partial ligand pyrolysis comprises two steps in the temperature range of 254–522 °C. The first one occurred within the range 254–364 °C with a weight loss of 31.8%, associated with the elimination of two molecules of NH_3 and HCN. The second step corresponds to a weight loss of 48.3% in the range 365–522 °C, implying the removal of two molecules of HSCN.

The partial ligand pyrolysis of the Cd(II) complex involves three steps. The first step was illustrated by a mass loss of 19.8% ascribed to the removal of two molecules of NH_3. The second thermal decomposition process took place in the temperature range of 270–306 °C with a weight loss of 27.1%. After that, two molecules of HSCN were released within the range of 307–479 °C with a weight loss of 42.9%.

The kinetic and thermodynamic parameters of decomposition processes of the complexes, namely, activation energy (ΔE), enthalpy (ΔH), entropy (ΔS), and Gibbs free energy change (ΔG), were calculated by the Coats–Redfern method[45,46] in the following forms:

$$\ln[1 - (1 - \alpha)^{1-n}/(1 - n)T^2] = M/T + B, \text{ for } n \neq 1 \quad (1)$$

Table 4 Kinetic parameters of prepared transition metal complexes

Compound	Step	n order	T (K)	A (S-1)	E (kJ mol^{-1})	ΔH (kJ mol^{-1})	ΔS (kJ mol^{-1})	ΔG (kJ mol^{-1})
Co(II) complex	1St	0.50	348	5.72×10^4	36.46	33.56	−0.11	73.32
	2nd	0.33	417	9.27×10^6	60.28	56.82	−0.12	107.69
	3rd	1.00	551	4.34×10^3	49.83	45.25	−0.18	148.89
	4th	1.00	751	1.63×10^8	135.02	128.78	−0.10	206.20
Ni(II) complex	1St	0.33	352	5.86×10^2	30.90	27.97	−0.22	105.46
	2nd	0.33	403	1.8×10^7	59.60	56.25	−0.11	103.06
	3rd	1.00	473	1.39×10^6	63.92	59.99	−0.13	125
	4th	1.00	561	3.94×10^6	71.38	66.72	−0.11	130.5
	5th	0.66	719	8.68×10^2	56.55	50.58	−0.20	196.77
Cu(II) complex	1St	1	338	1.34×10^8	55.17	52.36	−0.09	85.51
	2nd	0.50	462	1.37×10^4	45.23	41.39	−0.17	123.17
	3rd	1.00	548	5.84×10	30.90	26.35	−0.22	148.99
Cd(II) complex	1St	1.00	339	8.62×10^5	42.43	39.61	−0.14	87.123
	2nd	0.33	448	2.65×10^6	66.16	62.44	−0.13	122.04
	3rd	0	523	5.09×10^8	94.56	90.22	−0.09	137.64
	4th	0.50	561	2.26×10^6	77.69	73.02	−0.13	149.45
	5th	0.50	666	6.92×10^6	89.28	83.75	−0.12	169.25

$$\ln[-\ln(1-\alpha)/T^2] = M/T + \mathrm{B}, \text{ for } n = 1 \quad (2)$$

where $M = -E/R$ and $B = \ln AR/\Phi E$; R, A, and Φ are the universal gas constant, pre-exponential factor, and heating rate, respectively.

By plotting the left-hand side of eqn (1) or (2) *versus* $1000/T$ for different values of $n = 0$, 0.33, 0.50, 0.66, 1.00; the correlation coefficient, r, was calculated. The n value, which gave the best fit ($r \approx 1$), was chosen as the order parameter. The A and E values were determined from the intercept and linear slope of such stage. All other kinetic parameters, ΔH, ΔS, and ΔG, were obtained using the relationships; $\Delta H = E - RT$, $\Delta S = R[\ln(Ah/kT) - 1]$, and $\Delta G = \Delta H - T\Delta S$; k and h are the Boltzmann's constant and Plank's constant.

The thermo kinetic parameters of the decomposition steps for all complexes are collected in Table 4. The calculated data can be summarized with the following remarks:

(i) The activation energies of decomposition E are found to be in the range 30.90–135.02 kJ mol^{-1}. For all complexes except Ni(II) and Cu(II) complexes, the pattern of rising activation energy values is as follows: first stages, second stages, third stages. Also, the thermal stability of the complexes is demonstrated by the increasing positive values for E from one step to another.

(ii) The negative ΔS values for all complexes indicate that the activated complex is more ordered than the reactants and/or the reactions are slow.[47–49]

(iii) The positive values of ΔH imply that the decomposition processes are endothermic.

(iv) The relatively low and positive values of ΔG reveal the metal ion autocatalytic effect on the thermal decomposition of the complexes and non-spontaneous processes.[50] These data are confirmed with the calculated chemical potential (Table 2) (Section 3.2.)

3.4. Spectroscopic and magnetic studies

The spectroscopic techniques characterize the structure of transition metal complexes, and their spectroscopic analysis data reveal consistent results with the formulated data.

3.4.1. FT-IR spectra. For transition metal complexes, the most suggestive IR bands (4000–400 cm^{-1}) have been identified to provide useful information about **MCMT** ligand bonding sites when coordinated with metal ions. FT-IR spectra of transition metal complexes are provided in Fig. S3.† An analysis and comparison of the IR spectra of **MCMT** and its metal complexes suggest that **MCMT** behaves as a neutral bidentate ligand with azomethine–nitrogen and thione–sulfur as NS ligand. The presence of bands refers to the groups of hydrazine N–H and C=S, proposing the coordination of the **MCMT** ligand in a neutral form to the metal center. Also, the band attributable to C=S of the **MCMT** ligand (1235, 815 cm^{-1})[20] was shifted to lower wavenumbers (cm^{-1}) as a result of complex formation. The stretching vibration band of the azomethine group (HC=N) was also shifted to lower frequencies upon complexation. It was thought from first sight that these shifts could indicate the bonding of the unsaturated nitrogen of the azomethine group and thione-sulfur towards the metal ion.[51–53] The presence of new bands due to ν(M ← N) is at 470–478 cm^{-1} is another obvious sign of the participation of nitrogen atom of the azomethine group in the coordination.[54–56] The IR spectral data of the Co(II), Ni(II), and Cu(II) complexes show new bands at 3424–3440 cm^{-1} correlating to the overlap with lattice and/or coordinated water.[57] These bands are confirmed by the presence of non-ligand bands in the region of 544–545 cm^{-1} in the IR data of the complexes, which correspond to ν(M ← O).[58,59]

The stretching vibrations of NH_2, NH, and $(C{=}O)_{\gamma\text{-pyrone}}$ groups appeared nearly at the same position in the metal complexes compared to the free ligand as an indication of the non-participation of these groups in coordination.[60–63]

From above, the interpretation of experimental IR data is confirmed with theoretical results, which showed that the thiocarbohydrazone ligand during the coordination process acts as a neutral bidentate through its thione sulfur and imine nitrogen atoms. Moreover, the theoretical spectra for the studied metal complexes (in the most stable isomer; *all-trans*) were obtained using the computed vibrational frequencies along with their infrared intensities (see Fig. S3†). As a result, the predicted spectra (dashed lines) were found to closely match the experimental spectra (solid lines), particularly in the range below 1600 cm^{-1}, with minor discrepancies in the observed/calculated intensities.

3.4.2. ^{1}H-NMR spectra. ^{1}H-NMR spectral study also supported the formation of the thiocabohydrazone ligand. ^{1}H-NMR spectrum of the **MCMT** ligand (Fig. S4†) showed the following signals: 2.19 (s, 3H, CH_3), 4.19 (s, 2H, NH_2), 6.78–6.89 (m, 1H, H-8), 7.68–7.71 (m, 1H, H-7), 8.31 (s, 1H, H-5), 8.53 (s, 1H, CH=N),

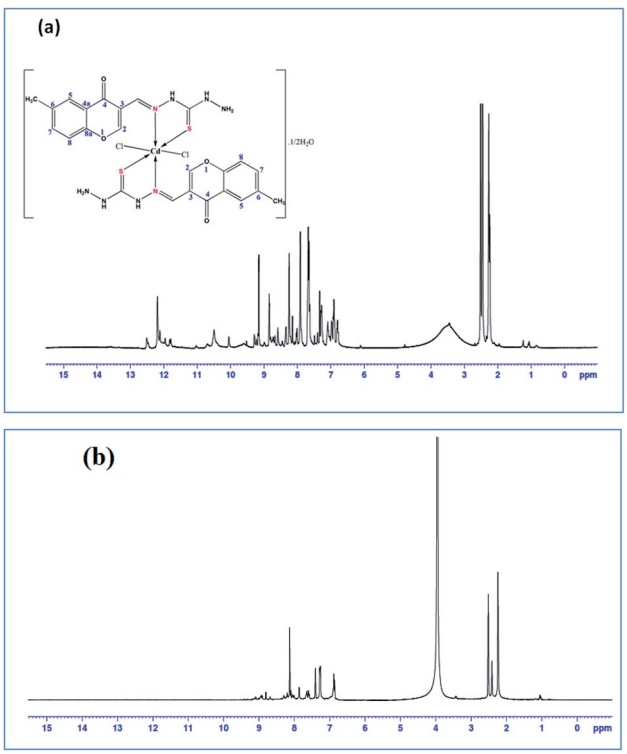

Fig. 5 ^{1}H-NMR spectra of Cd(II) complex in (a) DMSO-d_6 and (b) D_2O.

9.14 (s, 1H, H-2), 10.41 (s, 1H, NH), 12.09 (s, 1H, NH). In addition, the presence of a signal due to δNH protons in the spectrum of the ligand implies the ligand was present in the keto-form in the DMSO-d_6 solution.

The ^{1}H-NMR spectra of the Cd(II) diamagnetic complex relative to TMS in DMSO-d_6 without and with D_2O are represented in Fig. 5a and b. *Via* comparing the ^{1}H-NMR spectral data of the ligand with the corresponding data in the complex, the coordinating mode of the ligand was clarified. As shown in Fig. 5a, the ^{1}H-NMR spectrum of the Cd(II) complex shows peaks at 10.49 and 12.19 ppm relative to the NH of CS*NH* NH_2 and CH]N*NH* CS groups,[64–68] respectively, with the slightly upfield shift of two previous signals confirming the coordination of CH=N and C=S groups with metal ion and the **MCMT** ligand coordinating to the metal ion in neutral form. Also, the azomethine proton signals undergo an upfield shift after complexation. This is attributable to the nitrogen atoms of azomethine donating the lone pair of electrons to the central metal ion, resulting in a coordination linkage (M ← N).[69]

It is significant to observe the slightly upfield shift of NH_2 protons (3.88 ppm) in the spectrum of the diamagnetic complex compared with the NH_2 signal of **MCMT** ligand (4.12 ppm) due to the existence of strong hydrogen bonds in the free ligand. Also, the ^{1}H-NMR spectrum of the Cd(II) complex displays aromatic protons in the region of δ 6.77–9.15 ppm as complex multiplets.[70,71] On adding D_2O, the signals attributable to the protons of two NH groups were removed entirely while the other signals remained at the same locations. This statement was confirmed the infrared assignment.

3.4.3. Electronic spectra and magnetic moment. The electronic absorption spectra have been considered a helpful tool in the investigation. The UV-Vis spectra of the **MCMT** ligand and its related complexes clarified the coordinated geometry and estimated the intra ligand, ligand–metal, and d–d electronic transitions. A good description of the important electronic absorption spectral bands of the ligand and its complexes and an examination of the studies given by magnetic moment measurements are reported. The resultant UV-visible spectra of the metal complexes are presented in Fig. 6. The electronic spectral data of **MCMT** is characterized by the absorption bands at 270, 296, 316, 345, and 410 nm. The highest energy bands are assigned to π–π* transitions within aromatic rings.[69,70] Moderate energy bands can be assigned to n–π* transitions within C=O and C=N groups.[72–75] Upon complexation, the π–π* and n–π* transitions in all the metal complexes were changed. This reveals the strong coordination between the

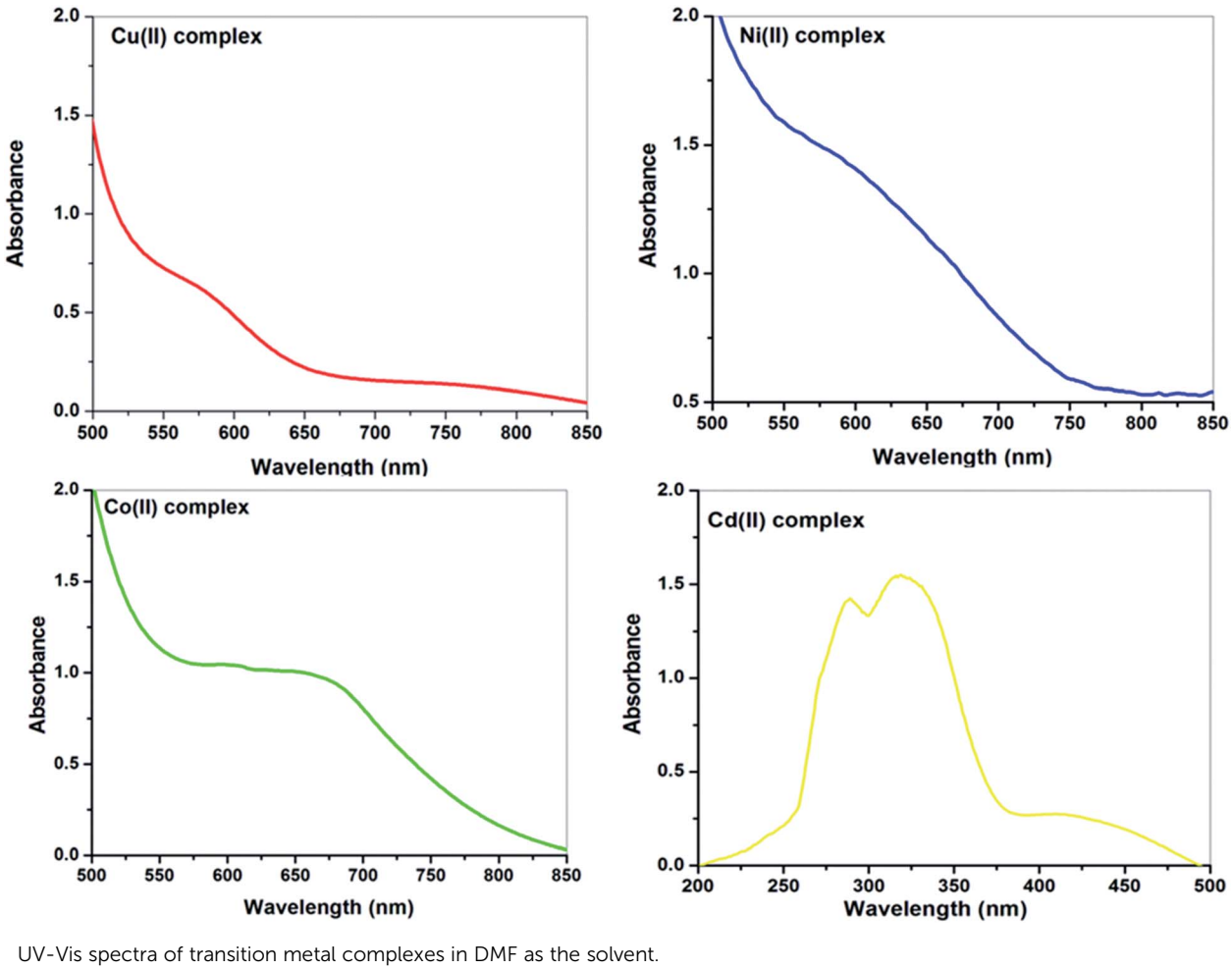

Fig. 6 UV-Vis spectra of transition metal complexes in DMF as the solvent.

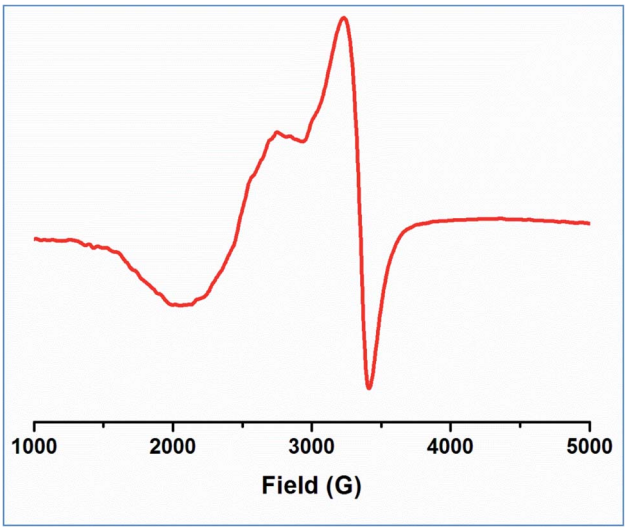

Fig. 7 ESR spectrum of Cu(II) complex.

metal ion and the **MCMT** ligand. The **LMCT** transitions are observed in the range of 415–451 nm.[75] The metal chelates showed additional absorption bands around 580–660 nm attributed to d–d transitions.[30]

The electronic spectrum of the Co(II) complex, in addition to magnetic moment measurements, illustrated that the complex has an octahedral geometry. The electronic transitions can be successfully explained using the Tanabe–Sugano diagram. In the octahedral Co(II) complexes, the spectra usually contain three bands.[76] The first band, which is ascribed to $^4T_{1g}(F) \rightarrow {}^4T_{2g}(F)$ transition, was not detected due to the fact that it lies in the near infra-red region and out of range of the used instrument. In the current work, only one broad band was observed in the visible region (660 nm), which may be due to the $^4T_{1g} \rightarrow {}^4A_{2g}(F)$ transition in an octahedral geometry.[77] The value of the room temperature magnetic moment of the Co(II) complex is 4.3 B.M, which agrees with the value of the octahedral geometry.[78]

Generally, the spectra of octahedral Ni(II) include three bands, which are assigned as $^3A_{2g}(F) \rightarrow {}^3T_{2g}(F)$, $^3A_{2g}(F) \rightarrow {}^3T_{1g}(F)$ and $^3A_{2g}(F) \rightarrow {}^3T_{1g}(P)$.[79] In the electronic spectrum of the complex, the first $^3A_{2g}(F) \rightarrow {}^3T_{2g}(F)$ transition was not observed due to the fact that it lies in the near infra-red and it is out of range of the used instrument. The spectrum of the current Ni(II) complex (Fig. 6) shows a broad absorption band at 585 nm, which is attributed to the $^3A_{2g}(F) \rightarrow {}^3T_{1g}(F)$ transition, in favor of octahedral geometry.[80] Also, the magnetic moment value of the Ni(II) complex confirmed the presence of two unpaired electrons in the octahedral geometry (2.90 B.M.).[80]

As a result of the Jahn–Teller distortion and the low symmetry of the environment around copper(II)-ion (d^9-system), complete interpretations of the electronic spectra and magnetic properties are rather complicated.[81] The electronic absorption spectrum of the Cu(II) complex showed a broad band in the visible region at 580 nm (Fig. 6). This band is assigned to $^2E_g \rightarrow {}^2T_{2g}$ transition in the distorted octahedral around Cu(II) complex.[82,83] The magnetic moment of the Cu(II) complex appeared at 1.8 B.M., which agrees with the value of the octahedral geometry.[84,85]

The yellow Cd(II) complex displayed absorption bands at 288, 318, and 415 nm that could be due to π–π*, n–π*, and CT transitions, respectively. The electronic spectrum of the Cd(II) complex does not include any specific evidence for

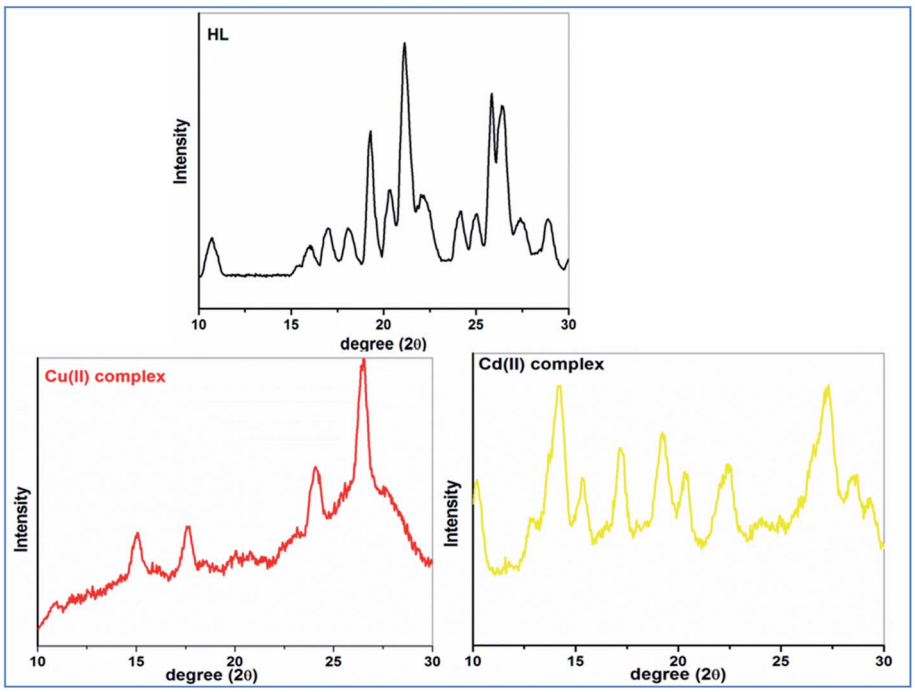

Fig. 8 XRD pattern of **MCMT**, Cu(II), and Cd(II) complexes.

stereochemistry, but octahedral geometry is proposed for the Cd(II) complex based on analytical, thermal, and infrared spectral evidence.

3.4.4. ESR spectra. ESR spectrum of the Cu(II) complex has been measured at room temperature, as shown in Fig. 7. The shape of ESR signals for the Cu(II) complex indicates octahedral geometry, where two anisotropic signals are observed. From the calculated g values of Cu(II) complex ($g_\perp = 2.06$ and $g_\parallel = 2.13$), it is obvious that $g_\parallel > g_\perp$ which indicates that the unpaired electron is predominantly in the $d_{x^2-y^2}$ orbital, giving $^2B_{1g}$ as the ground state. The observed data show that the $g_\parallel$ value > 2.0023, and hence the metal–ligand bonding essentially has a covalent character.[83] The geometric parameter G for the Cu(II) complex is 2.30, demonstrating a considerable exchange interaction in the solid complex. Molecular orbital coefficients, α^2 and β^2, were calculated.[58] The lower value of β^2 (0.44) compared to α^2 (0.79) indicates that the in-plane π-bonding is more covalent than the in-plane σ-bonding.[83]

3.4.5. X-ray diffraction (XRD) results. Powder XRD was measured for **MCMT** and its complexes. Fig. 8 shows the XRD patterns of the prepared **MCMT** and its Cu(II) and Cd(II) complexes as representative examples. XRD patterns showed that the crystals of the complexes are not ideal but lie between amorphous and crystalline characteristics. Because of this, the complexes were not found to be suitable for single crystal XRD. By observing the patterns of XRD of prepared **MCMT** and its Cu(II) and Cd(II) complexes, it is suggested that the Cu(II) and Cd(II) complexes exhibit crystalline character. It can be noted from the patterns that the diffraction angle and diffraction intensity of the prepared complexes differ from those of the ligand. This finding indicates that the metal ions have been bonded with the ligand to create new complexes.

The crystal sizes of the complexes were determined using the standard Scherer equation's maximal intensity peak.[86–88] The calculated values for the complexes **MCMT**, Cu(II), and Cd(II) were 16.6, 15.5, and 12.2 nm, respectively, suggesting nano-size of the crystals. Because of the extremely amorphous pattern of Ni(II) and Co(II) complexes, their crystal size could not be determined.

3.5. Optical study

The measured diffused reflectance (DR) was analyzed using the Kubelka–Munk (K–M) model, which illustrates the behavior of scattered light.[89] The product of the absorption coefficient α and sample thickness t is the K–M function $F(\mathrm{DR})$, which can be calculated as follows:[90,91]

$$F(\mathrm{DR}) = (\alpha t) = \frac{(1-\mathrm{DR})^2}{2\ \mathrm{DR}}$$

To determine the energy gap E_g, the absorption coefficient has been analyzed using the following equation:[92,93]

Table 5 Values of optical energy gaps of MCMT ligand and its transition metal complexes

Compound	Energy gap, [eV]
MCMT	1.65, 2.64, 2.96
Co(II) complex	1.54
Ni(II) complex	1.72, 2.06
Cu(II) complex	1.39, 2.00
Cd(II) complex	1.62, 2.37, 2.73

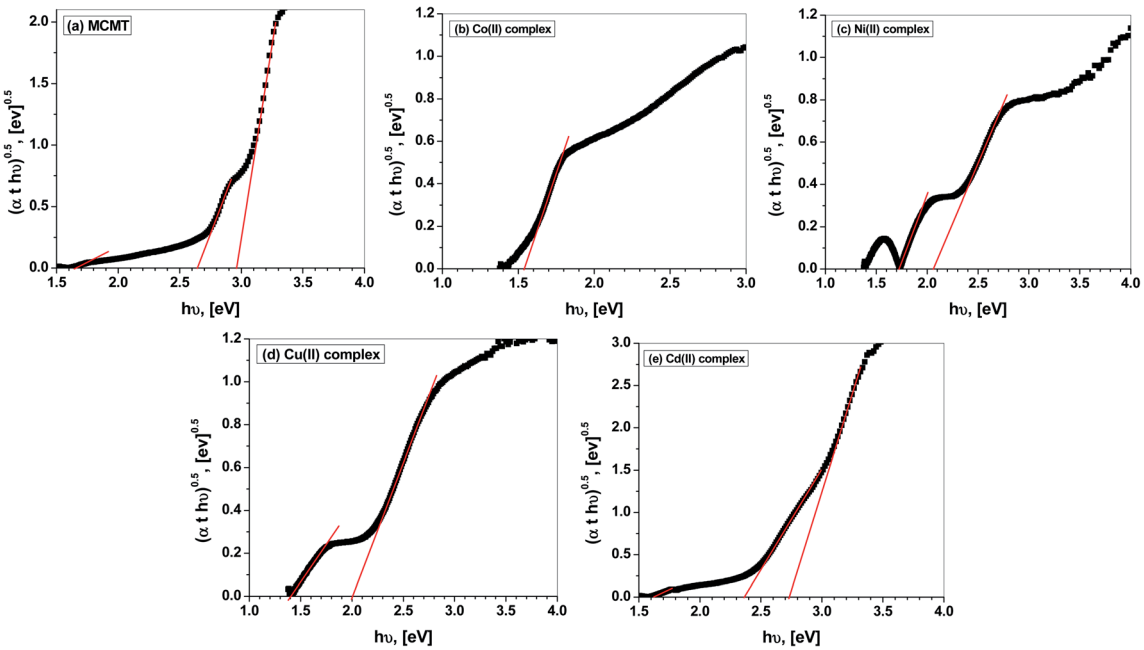

Fig. 9 $(\alpha th\nu)^{0.5}$ *versus* $h\nu$ of: (a) MCMT ligand; (b) Co(II) complex; (c) Ni(II) complex; (d) Cu(II) complex; (e) Cd(II) complex.

$$(\alpha thv) = At(hv - E_g)^m$$

where A is a constant and m is a number determining the type of optical transitions. $m = 2$ for indirect allowed transition while $m = 0.5$ for direct allowed transition. Fig. 9a–e show that $(\alpha thv)^{0.5}$ *versus* hv have regions with linear fitting. This indicates the indirect allowed optical transitions in the ligand and its complexes. The energy gaps have been determined from the extrapolation to the hv axis. Values of the energy gaps are presented in Table 5, showing the semi-conductive and proficient photovoltaic nature of the ligand and complexes.[94,95] The observed optical energy gap of 1.62 eV for the Cd(II) complex is in excellent agreement with that obtained theoretically (Table 2). On the other hand, the calculated values for Cu(II), Ni(II), and Co(II) complexes were found to be overestimated by 0.428–0.866 eV (Tables 2 and 5). These deviations could be attributed to the fact that the experimental value was obtained for the sample in the solid phase while the theoretical values were predicted for an isolated molecule of the complex ignoring the interactions in the solid state.

3.6. Electrical and dielectric properties

The ac electrical conductivity σ_{ac} of the ligand and its complexes has been calculated using the following equation:[96]

$$\sigma_{ac} = \frac{d}{ZA} - \frac{d}{RA}$$

where Z is the impedance, R is the resistance, d is the thickness, and A is the area. The frequency dependence of ac conductivity is presented in Fig. 10. It is clear that σ_{ac} for all samples increases linearly with frequency. This is a common feature for semiconducting materials where increasing the frequency promotes electronic jumps between localized states and increases the mobility of charge carriers.[96,97] Clearly, the Cu(II) complex has higher ac conductivity than the ligand while Ni(II), Co(II), and Cd(II) complexes have lower ac conductivities. This behavior is similar to the Cu(II) complex derived from acyclovir (ACV).[98] The higher ac conductivity of the Cu(II) complex can be assigned to: (i) the Cu(II) complex has higher coordination energy based on theoretical calculations, and thus strong coordination power between ligand and Cu(II) ion, consequently, implying that the Cu(II) metal ion in the Π-electron delocalization of the organic molecule during complexation leads to decreasing the energy gap and increment the electrical conductivity; (ii) the high crystallinity of the Cu(II) complex as discussed in the XRD section. The ligand has higher ac conductivity than that of Ni(II) and Co(II) complexes due to its high crystallinity while Ni(II) and Co(II) complexes have an amorphous structure. Also, keto–enol transformation is known to occur in such ligand, which implies the movement of Π-electrons along the ligand (*i.e.*, delocalization), which prompts the increment of electrical conductivity. On the other hand, the low ac conductivity of the Cd(II) complex may be attributed to the absence of free unpaired electrons. Also, the Cu(II)complex has the highest ac conduction response to the frequency. This is a promising feature to be a potential applicant for electronic applications. The frequency dependence has been analyzed using the following Jonscher's universal power equation:[99,100]

$$\sigma_{ac} = B(2\pi f)^S$$

where B is a constant. The frequency exponent S determines the mechanism of the ac conduction. Fig. 11 presents $\ln\sigma_{ac}$ *versus* $\ln(2\pi f)$ for all complexes. The slope of both lines (S) is close to unity, as seen in Table 6. This behavior contradicts the Quantum Mechanical Tunneling (QMT) model,[101,102] which predicts the value for S to be about 0.81. Thus, the ac conduction in these complexes could be explained as correlated barrier hopping (CBH).

The CBH model considered a simultaneous hopping of two electrons between close pairs of centers (negatively and

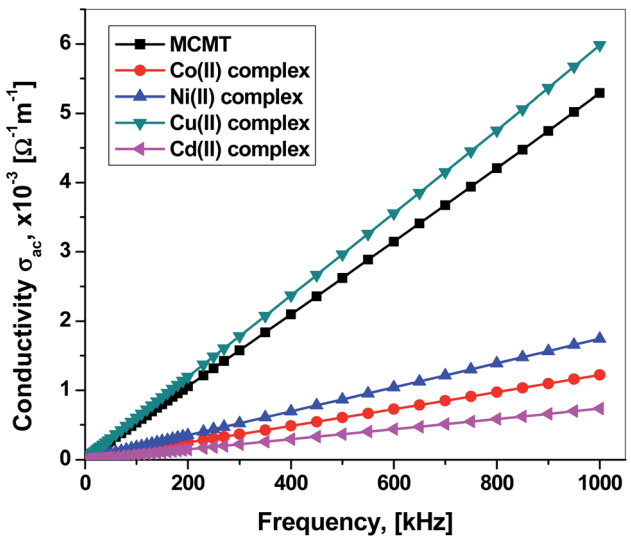

Fig. 10 Frequency dependence of the ac conductivity for MCMT and Co(II), Ni(II), Cu(II), and Cd(II) complexes.

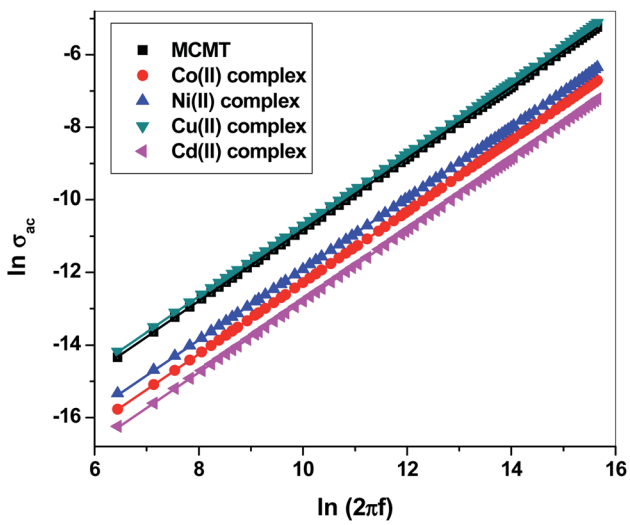

Fig. 11 ln σ_{ac} *versus* ln(2π*f*) for MCMT and Co(II), Ni(II), Cu(II), and Cd(II) complexes.

Table 6 Values of the frequency exponent and maximum barrier height (W_m)

Compound	S	W_m
MCMT	0.9824	2.9850
Co(II) complex	0.9815	2.8399
Ni(II) complex	0.9764	2.2311
Cu(II) complex	0.9819	2.9010
Cd(II) complex	0.9809	2.7507

positively charged centers) over a barrier height, and these two centers are correlated with inter-site separation (5–10 Å apart) *via* the coulombic interaction. When all the charged, spin-paired defect centers in the materials are associated into close pairs, the pairs could be with intimate or random distribution. So, the CBH could happen between intimate valence alternation pairs (IVAP) or non-intimate valence alternation pairs (NVAP), respectively. The frequency exponent S is temperature dependent with values less than 1, while S is very close to unity in IVAP. Thus, the ac conduction in these complexes could be explained as correlated barrier hopping (CBH) between intimate valence alternation pairs (IVAP).[103,104] The maximum barrier height (W_m) in this model can be calculated using the following equation:[105]

$$W_m = \frac{2k_B T}{1 - S}$$

Values of W_m are presented in Table 6. Clearly, the Ni(II) complex has the lowest maximum barrier height.

Fig. 12 shows the frequency dependence of the dielectric constant ε_1 for the studied complexes. Clearly, the Cu(II) complex has a higher dielectric constant than the ligand, while Ni(II), Co(II), and Cd(II) complexes have a lower dielectric constant. At low frequencies, ε_1 decreases sharply with

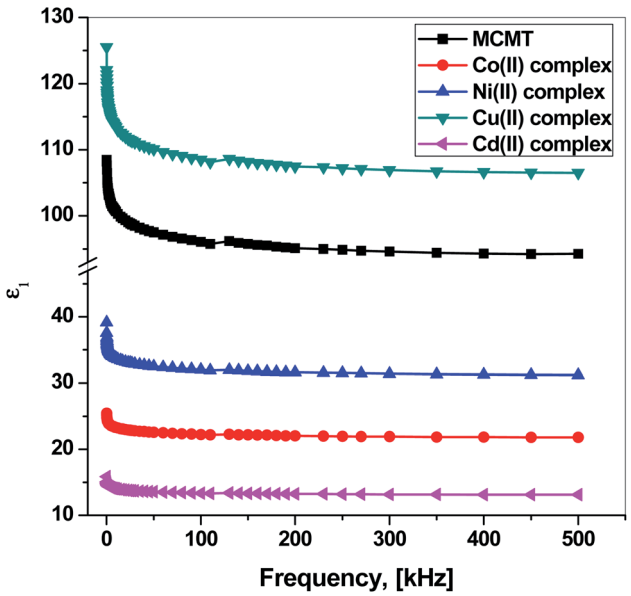

Fig. 12 Frequency dependence of the dielectric constant ε_1 for MCMT, Co(II), Ni(II), Cu(II), and Cd(II) complexes.

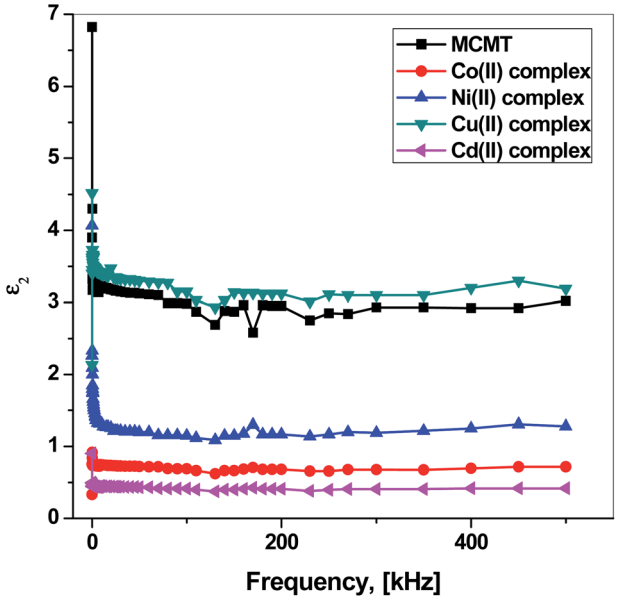

Fig. 13 Frequency dependence of the dielectric loss ε_2 for MCMT, Co(II), Ni(II), Cu(II), and Cd(II) complexes.

increasing frequency for all the complexes. Then, ε_1 decreases gradually with increasing frequency. At high frequencies, ε_1 decreases slightly. When the sample is placed in an alternating electric field, the dielectric properties can be interpreted by considering a set of dipoles. The dielectric constant represents the degree of polarization of the material and its ability to store the electric field.[106] Thus, Cu(II) complex is considered to have the highest polarization and storage ability.

At low frequencies, the dielectric constant ε_1 for the polar material is due to the contribution of multicomponent of polarizability, deformational polarization (electronic and ionic polarization), and relaxation polarization (orientation and interfacial polarization).[107] When the frequency is increased, the dipoles will no longer be able to rotate rapidly, so that their oscillations begin to lag behind those of the field. So, the orientation and ionic contribution decreases, leading to decreasing ε_1.[108] As the frequency is further increased, the dipole will be unable to follow the field completely, stopping the orientation and ionic polarization. Thus, ε_1 approaches approximately to a constant value at higher frequencies due to the interfacial contribution only.[97]

Fig. 13 shows the frequency dependence of the dielectric loss ε_2, which represents the dissipation of energy.[106] Clearly, the Cu(II) complex has the highest dissipation of energy, while Cd(II) complex has the lowest dissipation of energy. At low frequencies, ε_2 is high and decreases with increasing frequency. Then, it starts to decrease slightly with some fluctuation. At lower frequencies, the high values of ε_2 is due to many sources such as ion jump, conduction loss of charge carriers, ion polarization, and ion vibration. At higher frequencies, the ion vibrations could be the only source for the dielectric loss.[97]

4. Conclusion

The current paper introduced the synthesis, structure, and physicochemical properties of the new complexes of Co(II), Ni(II), Cu(II), and Cd(II) ions with (1*E*)-1-((6-methyl-4-oxo-4*H*-chromen-3-yl)methylene)thiocarbonohydrazide ligand (**MCMT**). The **MCMT** was able to form complexes with metal ions by coordination through N and S atoms. The complexes are formed in 1 : 2 (ML_2) ratio and exhibit octahedral geometry. The crystal study indicates that the complexes are in nanodomain. The results of DFT-B3LYP calculations are found to be in good agreement with the infrared spectral analysis, and the complexes prefer the *all trans* geometrical isomer with coordination stability in the order of Cu(II) > Ni(II) > Co(II). The ligand and its complexes have indirect allowed optical transitions. Frequency response of the AC conductivity of the ligand and its complexes refers to correlated barrier hopping between intimate valence alternation pairs. Cu(II) complex has the highest response for the AC conductivity to the frequency and the highest polarization and storage ability.

Conflicts of interest

The authors declare that they have no known competing financial interests or personal relationships that could have appeared to influence the work reported in this paper.

Acknowledgements

The authors extend their appreciation to the Deanship of Scientific Research at King Khalid University for funding this work through a research group program under grant number RGP.1/5/42.

References

1 V. M. Leovac, S. A. B. Novakovic, M. D. Joksovic, G. A. Bogdanovic, K. M. Szecsenyi and V. I. Cesljevic, Transition metal complexes with thiosemicarbazide-based ligands. Part LVI: Nickel(II) complex with 1,3-diphenylpyrazole-4-carboxaldehyde thiosemicarbazone and unusually deformed coordination geometry, *Polyhedron*, 2007, **26**, 3783, DOI: 10.1016/j.poly.2007.04.012.

2 M. Joseph, E. Suresh, M. Kuriakose, M. R. P. Kurup, A. Kishore and S. G. Bhat, Structural, antimicrobial and spectral studies of copper(II) complexes of 2-benzoylpyridine N(4)-phenyl thiosemicarbazone, *Polyhedron*, 2006, **25**, 61, DOI: 10.1016/j.poly.2005.07.006.

3 S. E. Bakir, M. Sahin, M. Zahoor, E. D. Portakal and B. Ülküseven, Synthesis and biological potentials of dioxomolybdenum(VI) complexes with ONS and ONN chelating thiosemicarbazones: DNA-binding, antioxidant and enzyme inhibition studies, *Polyhedron*, 2020, **190**, 114754, DOI: 10.1016/j.poly.2020.114754.

4 U. M. Osman, S. Silvarajoo, K. H. Kamarudin, M. I. M. Tahir and H. C. Kwong, Ni(II) Complex containing a thiosemicarbazone ligand: Synthesis, spectroscopy, single-crystal X-ray crystallographic and conductivity studies, *J. Mol. Struct.*, 2021, **1223**, 128994, DOI: 10.1016/j.molstruc.2020.128994.

5 M. Shebl, S. M. E. Khalil and F. S. Al-Gohani, J. Mol. Struct. Preparation, spectral characterization and antimicrobial activity of binary and ternary Fe(III), Co(II), Ni(II), Cu(II), Zn(II), Ce(III) and UO_2(VI) complexes of a thiocarbohydrazone ligand, *J. Mol. Struct.*, 2010, **980**, 78, DOI: 10.1016/j.molstruc.2010.06.040.

6 J. C. Logan, M. P. Fox, J. H. Morgan, A. M. Makhon and C. J. Pfau, Arenavirus inactivation on contact with N-substituted isatin beta-thiosemicarbazones and certain cations, *J. Gen. Virol.*, 1975, **28**, 271, DOI: 10.1099/0022-1317-28-3-271.

7 A. S. Dobek, D. L. Klayman, E. J. Dickson Jr, J. P. Scovill and E. C. Tramont, Inhibition of clinically significant bacterial organisms in vitro by 2-acetylpyridine thiosemicarbazones, *Antimicrob. Agents Chemoether.*, 1980, **18**, 27.

8 R. Vikneswaran, N. E. Eltayeb, S. Ramesh and R. Yahya, New alicyclic thiosemicarbazone chelated zinc (II) antitumor complexes: Interactions with DNA/protein, nuclease activity and inhibition of topoisomerase-I, *Polyhedron*, 2016, **105**, 89, DOI: 10.1128/aac.18.1.27.

9 M. Wehbe, A. W. Y. Leung, M. J. Abrams, C. Orving and M. B. Bally, A Perspective can copper complexes be developed as a novel class of therapeutics, *Dalton Trans.*, 2017, **46**, 10758, DOI: 10.1039/c7dt01955f.

10 Y.-H. Liu, A. Li, J. Shao, C.-Z. Xie, X.-Q. Song, W.-G. Bao and J. Yu Xu, Cadmium(ii) complexes with a 4-acyl pyrazolone derivative and co-ligands: crystal structures and antitumor activity, *Dalton Trans.*, 2016, **45**, 8036, DOI: 10.1039/c6ra23938b.

11 F. A. Beckford, J. Thessing, M. Shaloski Jr, P. C. Mbarushimana, A. Brock, J. Didion, J. Woods, A. Gonzalez-Sarrías and N. P. Seeram, Synthesis and characterization of mixed-ligand diimine-piperonal thiosemicarbazone complexes of ruthenium(II): biophysical investigations and biological evaluation as anticancer and antibacterial agents, *J. Mol. Struct.*, 2011, **992**, 39, DOI: 10.1016/j.molstruc.2011.02.029.

12 T. Bakir, H. S. Sayiner and F. Kandemirli, Experimental and theoretical investigation of antioxidant activity and capacity of thiosemicarbazones based on isatin derivatives, Phosphorus, Sulfur, *Silicon Relat. Elem.*, 2018, **193**, 494, DOI: 10.1080/10426507.2018.1452232.

13 H. Beraldo and D. Gambinob, The Wide Pharmacological Versatility of Semicarbazones, Thiosemicarbazones and Their Metal Complexes, *Mini-Rev. Med. Chem.*, 2004, **4**, 31, DOI: 10.2174/1389557043487484.

14 F. Bacher, O. Dömötör, A. Chugunova, N. V. Nagy, L. Filipovi, S. Radulovic, E. A. Enyedy and V. B. Arion, Strong effect of copper(ii) coordination on antiproliferative activity of thiosemicarbazone–piperazine and thiosemicarbazone–morpholine hybrids, *Dalton Trans.*, 2015, **44**, 9071, DOI: 10.1039/c5dt01076d.

15 S. Singh, P. K. Mandal, N. Singh, A. K. Misra, S. Singh, V. Chaturvedi, S. Sinha and A. K. Saxena, Substituted hydrazinecarbothioamide as potent antitubercular agents: synthesis and quantitative structure-activity relationship (QSAR), *Bioorg. Med. Chem. Lett.*, 2010, **20**, 2597, DOI: 10.1016/j.bmcl.2010.02.081.

16 U. M. Osman, S. Silvarajoo, K. H. Kamarudin, M. I. M. Tahir and H. C. Kwong, Ni(II) complex containing a thiosemicarbazone ligand: Synthesis, spectroscopy, single-crystal X-ray crystallographic And conductivity studies, *J. Mol. Struct.*, 2021, **1223**, 128994, DOI: 10.1016/j.molstruc.2020.128994.

17 A. H. Ahmed and M. G. Moustafa, Spectroscopic, morphology and electrical conductivity studies on Co(II), Ni(II), Cu(II) and Mn(II)-oxaloyldihydrazone complexes, *J. Saui Chem. Society*, 2020, **24**, 381, DOI: 10.1016/j.jscs.2020.02.003.

18 E. S. Scott and L. F. Audrieth, Hydrazine derivatives of the carbonic and thiocarbonic acids. II. Derivatives of thiocarbohydrazide, *J. Org. Chem.*, 1954, **19**, 742, DOI: 10.1021/jo01370a007.

19 H. M. El-Shaaer, P. Foltinova, M. Lacova, J. Chovancova and H. Stankovicova, Synthesis, antimicrobial activity and bleaching effect of TED some reaction products of 4-oxo-4H-benzopyran-3-carboxaldehydes with aminobenzothiazoles and hydrazides, *IL Farmaco*, 1998, **53**, 227, DOI: 10.1016/s0014-827x(98)00015-9.

20 T. E. Ali, S. A. Abdel-Aziz, H. M. El-Shaaer, F. I. Hanafy and A. Z. El-Fauomy, Synthesis of Bioactive 4-Oxo-4H-Chromenes Bearing Heterocyclic Systems from Hydrazonecarbodithioic Acid and Thiocarbohydrazone, Phosphorus, Sulfur, *Silicon Relat. Elem.*, 2008, **183**, 2139, DOI: 10.1080/10426500701851291.

21 A. D. Becke, Density-functional exchange-energy approximation with correct asymptotic behavior, *Phys. Rev. A*, 1988, **38**, 3098, DOI: 10.1103/physreva.38.3098.

22 C. Lee, W. Yang and R. G. Parr, Development of the Colle-Salvetti correlation-energy formula into a functional of the electron density, *Phys. Rev. B*, 1988, **37**, 785, DOI: 10.1103/physrevb.37.785.

23 S. Niu and M. B. Hall, Theoretical studies on reactions of transition-metal complexes, *Chem. Rev.*, 2000, **100**, 353, DOI: 10.1021/cr980404y.

24 H. Paulsen, L. Duelund, H. Winkler, H. Toftlund and A. X. Trautwein, Free energy of spin-crossover complexes calculated with density functional methods, *Inorg. Chem.*, 2001, **40**, 2201, DOI: 10.1021/ic000954q.

25 J. N. Harvey, On the accuracy of density functional theory in transition metal chemistry, *Annu. Rep. Prog. Chem., Sect. C: Phys. Chem.*, 2006, **102**, 203, DOI: 10.1039/b419105F.

26 M. Bühl and H. Kabrede, Geometries of transition-metal complexes from density-functional theory, *J. Chem. Theory Comput.*, 2006, **2**, 1282, DOI: 10.1021/ct6001187.

27 P. J. Hay and W. R. Wadt, Ab initio effective core potentials for molecular calculations. Potentials for the transition metal atoms Sc to Hg, *J. Chem. Phys.*, 1985, **82**, 270, DOI: 10.1063/1.448799.

28 M. J. Frisch, G. W. Trucks, H. B. Schlegel, G. E. Scuseria, M. A. Robb, J. R. Cheeseman, G. Scalmani, V. Barone, B. Mennucci, G. A. Petersson, H. Nakatsuji, M. Caricato, X. Li, H. P. Hratchian, A. F. Izmaylov, J. Bloino, G. Zheng, J. L. Sonnenberg, M. Hada, M. Ehara, K. Toyota, R. Fukuda, J. Hasegawa, M. Ishida, T. Nakajima, Y. Honda, O. Kitao, H. Nakai, T. Vreven, J. A. Montgomery Jr, J. E. Peralta, F. o. Ogliaro, M. J. Bearpark, J. Heyd, E. N. Brothers, K. N. Kudin, V. N. Staroverov, R. Kobayashi, J. Normand, K. Raghavachari, A. P. Rendell, J. C. Burant, S. S. Iyengar, J. Tomasi, M. Cossi, N. Rega, N. J. Millam, M. Klene, J. E. Knox, J. B. Cross, V. Bakken, C. Adamo, J. Jaramillo, R. Gomperts, R. E. Stratmann, O. Yazyev, A. J. Austin, R. Cammi, C. Pomelli, J. W. Ochterski, R. L. Martin, K. Morokuma, V. G. Zakrzewski, G. A. Voth, P. Salvador, J. J. Dannenberg, S. Dapprich, A. D. Daniels, d. n. Farkas, J. B. Foresman, J. V. Ortiz, J. Cioslowski and D. J. Fox, *Gaussian 09*, Gaussian, Inc., Wallingford, CT, USA, 2009.

29 P. Pulay, Ab initio calculation of force constants and equilibrium geometries in polyatomic molecules, *Mol. Phys.*, 1969, **17**, 197, DOI: 10.1080/00268976900100941.

30 S. A. AbouEl-Enein, S. M. Emam, R. M. Wagdy and F. I. Abouzayed, Spectral and thermal investigation of novel biologically active (N-(1dimethyl-3-oxo-2-phenyl-2,3-dihydro-1H-pyrazol-4-yl)-2-(1,5dimethyl-3-oxo-2-phenyl-2,3-dihydro-1H-pyrazol-4-yl-amino)-2oxo-cetimidic acid) ligand and its metal complexes, *J. Mol. Struct.*, 2020, **1215**, 128230, DOI: 10.1016/j.molstruc.2020.128230.

31 H. F. El-Shafiy and M. Shebl, Binuclear oxovanadium(IV), cerium(III) and dioxouranium(VI) nano complexes of a bis(bidentate) ligand: Synthesis, spectroscopic, thermal, DFT calculations and biological studies, *J. Mol. Struct.*, 2019, **1194**, 187, DOI: 10.1016/j.molstruc.2019.05.063.

32 S. M. E. Khalil, M. Shebl and F. S. Al-Gohani, Zinc(II) thiosemicarbazone complex as a ligand towards some transition metal ions: Synthesis, spectroscopic and Antimicrobial Studies, *Acta Chim. Slov.*, 2010, **57**, 716.

33 H. S. Seleem, B. A. El-Shetary and M. Shebl, Synthesis and characterization of a novel series of metallo-thiocarbohydrazone polymers and their adducts, *Heteroat. Chem.*, 2007, **18**, 100, DOI: 10.1002/hc.20239.

34 U. C. Singh and P. A. Kollman, An approach to computing electrostatic charges for molecules, *J. Comput. Chem.*, 1984, **5**, 29, DOI: 10.1002/jcc.540050204.

35 B. H. Besler, K. M. Merz Jr and P. A. Kollman, Atomic charges derived from semiempirical methods, *J. Comput. Chem.*, 1990, **11**, 431, DOI: 10.1002/jcc.540110404.

36 A. D. Burrows, R. W. Harrington, M. F. Mahon and S. J. Teat, Manipulation of Molecular and Supramolecular Structure in Nickel(II) Complexes through the Orientation of Dicarboxylate Hydrogen Bonding Faces, *Cryst. Growth Des.*, 2004, **4**, 813, DOI: 10.1021/cg049930a.

37 K. C. Zheng, J. P. Wang, Y. Shen, W. L. Peng and F. C. Yun, Studies on electronic structures and related properties of complexes M(tap)32+ (M = Fe, Ru, Os) by the DFT

method, *J. Chem. Soc., Dalton Trans.*, 2002, **111**, 111, DOI: 10.1039/b105266g.

38 K. C. Zheng, X. W. Liu, J. P. Wang, F. C. Yun and L. N. Ji, DFT studies on the molecular orbitals and related properties of $[Ru(phen)_2(9,9'\text{-}2R\text{-}dpq)]^{2+}$(R=$NH_2$,OH,H and F), *J. Mol. Struct.: THEOCHEM*, 2003, **637**, 195, DOI: 10.1016/S0166-1280(03)00539-6.

39 H. Irving and R. J. P. Williams, The stability of transition-metal complexes, *J. Chem. Soc.*, 1953, **637**, 3192, DOI: 10.1039/jr9530003192.

40 T. Koopmans, Über die Zuordnung von Wellenfunktionen und Eigenwerten zu den Einzelnen Elektronen Eines Atoms, *Physica*, 1934, **1**, 104, DOI: 10.1016/S0031-8914(34)90011-2.

41 R. G. Parr, L. v. Szentpály and S. Liu, Electrophilicity Index, *J. Am. Chem. Soc.*, 1999, **121**, 1922, DOI: 10.1021/ja983494x.

42 Z. Zhou and R. G. Parr, Activation hardness: new index for describing the orientation of electrophilic aromatic substitution, *J. Am. Chem. Soc.*, 1990, **112**, 5720, DOI: 10.1021/ja00171a007.

43 L. Padmaja, C. Ravikumar, D. Sajan, I. Hubert Joe, V. S. Jayakumar, G. R. Pettit and O. F. Nielsen, Density functional study on the structural conformations and intramolecular charge transfer from the vibrational spectra of the anticancer drug combretastatin-A2, *J. Raman Spectrosc.*, 2009, **40**, 419, DOI: 10.1002/jrs.2145.

44 T. S. Xavier and I. H. Joe, FT-IR, Raman and DFT study of 2-amino-5-fluorobenzoic acid and its biological activity with other halogen (Cl, Br) substitution, *Spectrochimica Acta Part A*, 2011, **79**, 332, DOI: 10.1016/j.saa.2011.02.037.

45 A. W. Coats and J. P. Redfern, Kinetic parameters from thermogravimetric data, *Nature*, 1964, **201**, 68.

46 D. W. Johnson and P. K. Gallagher, Comparison of dynamic with isothermal techniques for the study of solid state decomposition kinetics, *J. Phys. Chem.*, 1972, **76**, 1474.

47 A. A. Frost and R. G. Pearson, *Kinetics andMechanism*, JohnWiley, New York, 1961.

48 S. A. Sadeek and W. H. El-Shwiniy, Preparation, structure and microbial evaluation of metal complexes of the second generation quinolone antibacterial drug lomefloxacin, *J. Mol. Struct.*, 2010, **981**, 130, DOI: 10.1016/j.molstruc.2010.07.041.

49 W. H. Mahmoud, G. G. Mohamed and M. M. I. El-Dessouky, Coordination modes of bidentate lornoxicam drug with some transition metal ions. Synthesis, characterization and in vitro antimicrobial and antibreastic cancer activity studies, *Spectrochim. Acta, Part A*, 2014, **122**, 598, DOI: 10.1016/j.saa.2013.11.069.

50 U. El-Ayaan and I. M. Gabr, Thermal, spectroscopic, and solvent influence studies on mixed-ligand copper(II) complexes containing the bulky ligand: Bis[N-(p-tolyl) imino]acenaphthene, *Spectrochim. Acta, Part A*, 2007, **67**, 263, DOI: 10.1016/j.saa.2006.07.012.

51 R. Fouad, Synthesis and Fundamental Characterization of Diverse Properties of Biocompatible Cd (II) Phosphor Complex for Cytotoxic Activity and Latent Fingerprint Detection, *Appl. Organomet. Chem.*, 2020, **34**, 5497, DOI: 10.1002/aoc.5497.

52 G. Kalaiaras, S. R. J. Rajkuma, S. Dharani, V. M. Lynch and R. Prabhakaran, Synthesis, spectral characterization and biological evaluation of some copper(II) complexes containing 4-oxo-4H-chromene-3-carbaldehyde-4-(N)-substituted thiosemicarbazones, *Inorg. Chim. Acta*, 2018, **471**, 759, DOI: 10.1016/j.ica.2017.12.008.

53 M. Shebl, M. A. Ibrahim, S. M. E. Khalil, S. L. Stefan and H. Habib, Binary and ternary copper(II) complexes of a tridentate ONS ligand derived from 2-aminochromone-3 carboxaldehyde and thiosemicarbazide: Synthesis, spectral studies and antimicrobial activity, *Spectrochim. Acta, Part A*, 2013, **115**, 399, DOI: 10.1016/j.saa.2013.06.075.

54 M. Shebl, Synthesis and spectroscopic studies of binuclear metal complexes of a tetradentate N_2O_2 Schiff base ligand derived from 4,6-diacetylresorcinol and benzylamine, *Spectrochim. Acta, Part A*, 2008, **70**, 850, DOI: 10.1016/j.saa.2007.09.035.

55 O. M. I. Adly and A. Taha, Coordination diversity of new mononuclear ONS hydrazone with transition metals: Synthesis, characterization, molecular modeling and antimicrobial studies, *J. Mol. Struct.*, 2013, **1038**, 250, DOI: 10.1016/j.molstruc.2013.01.035.

56 M. Shebl and S. M. E. Khalil, synthesis, spectral, X-ray diffraction, antimicrobial studies, and DNA binding properties of binary and ternary complexes of pentadentate N_2O_3 carbohydrazone ligands, *Monatsh. Chem.*, 2015, **146**, 15, DOI: 10.1007/s00706-014-1302-x.

57 M. Shebl, synthesis, spectral studies, and antimicrobial activity of binary and ternary Cu(II), Ni(II), And Fe(III) complexes of new hexadentate Schiff bases derived from 4,6-diacetylresorcinol and amino acids, *J. Coord. Chem.*, 2009, **62**, 3217, DOI: 10.1080/00958970903012785.

58 M. Saif, M. M. Mashaly, M. F. Eid and R. Fouad, Synthesis and thermal studies of tetraaza macrocylic ligand and its transition metal complexes. DNA binding affinity of copper complex, *Spectrochim. Acta, Part A*, 2011, **79**, 1849, DOI: 10.1016/j.saa.2011.05.071.

59 M. Saif, M. M. Mashaly, M. F. Eid and R. Fouad, Synthesis, characterization and thermal studies of binary and/or mixed ligand complexes of Cd(II), Cu(II), Ni(II) and Co(III) based on 2-(Hydroxybenzylidene) thiosemicarbazone: DNA binding affinity of binary Cu(II) complex, *Spectrochim. Acta, Part A*, 2012, **92**, 347, DOI: 10.1016/j.saa.2012.02.098.

60 K. S. Abou Melha, In-vitro antibacterial, antifungal activity of some transition metal complexes of thiosemicarbazone Schiff base (HL) derived from N4-(7'-chloroquinolin-4'-ylamino) thiosemicarbazide, *J. Enzyme Inhib. Med. Chem.*, 2008, **23**, 493, DOI: 10.1080/14756360701631850.

61 A. A. A. Abou-Hussein and W. Linert, Synthesis, spectroscopic and biological activities studies of acyclic and macrocyclic mono and binuclear metal complexes containing a hard-soft Schiff base, *Spectrochim. Acta, Part A*, 2012, **95**, 596, DOI: 10.1016/j.saa.2012.04.057.

62 Y. Li, Z.- Yin Yang and J. Cai Wu, Synthesis, crystal structures, biological activities and fluorescence studies of

transition metal complexes with 3-carbaldehyde chromone thiosemicarbazone, *Eur. J. Med. Chem.*, 2010, **45**, 5692, DOI: 10.1016/j.ejmech.2010.09.025.

63 G. Prakash, S. Selvamurugan, R. Ramachandran, P. Vijayan, R. Manikandan, A. Endo, P. Viswanathamurthi, K. Velmurugan and R. Nandhakumar, Synthesis, crystal structure and biological evaluation of Ni(II) complexes containing 4-chromone-N(4)-substituted thiosemicarbazone ligands, *Polyhedron*, 2016, **107**, 57, DOI: 10.1016/j.poly.2016.01.011.

64 K. G. Sangeetha and K. K. Aravindakshan, Novel ligands, benzophenone N(4)-methyl-N(4) phenylthiosemicarbazone,1-(amino-N-methylphenylmethanethio) (diphenylmethylene) thiocarbonohydrazide and the transition metal complexes of the latter, *Inorg. Chim. Acta*, 2018, **469**, 387, DOI: 10.1016/j.ica.2017.09.057.

65 S. K. Padhan, J. Palei, P. Rana, N. Murmu and S. N. Sahu, Sequential displacement strategy for selective and highly sensitive detection of Zn^{2+}, Hg^{2+} and S^{2-} ions: An approach toward a molecular keypad lock, *Spectrochim. Acta, Part A*, 2019, **208**, 271, DOI: 10.1016/j.saa.2018.10.016.

66 A. Rai, N. Kumari, A. K. Srivastava and L. Mishra, Synthesis and characterization of bispentafluorophenyl carbohydrazone/thiocarbohydrazone: selective recognition of F^- ions, *Tetrahedron Lett.*, 2013, **54**, 7151, DOI: 10.1016/j.tetlet.2013.10.100.

67 E. Subasi, H. A. Kayali, E. B. Atalay, D. Erdogan, B. Sen and B. Pakyapan, Synthesis and characterization of thiosemicarbazone-functionalized organoruthenium (II)-arene complexes: Investigation of antitumor characteristics in colorectal cancer cell lines, *Mat. Sci. Engin. C*, 2020, **106**, 110152, DOI: 10.1016/j.msec.2019.110152.

68 L. Dkhar, M. R. Kollipara, V. Banothu, K. M. Poluri and W. Kaminsky, Platinum group complexes containing salicylaldehyde based thiosemicarbazone ligands: Their synthesis, characterization, bonding modes, antibacterial and antioxidant studies, *J. Organomet. Chem.*, 2020, **918**, 121298, DOI: 10.1016/j.jorganchem.2020.121298.

69 B. I. Ceylan, Y. Kurt, O. Bolukbasi, A. Yilmaz, K. Kaya and B. Ülküseven, Synthesis, spectroscopic characterization and quantum chemical studies of a dioxomolybdenum(VI) complex with an N,Substituted pyridoxal thiosemicarbazone, *Polyhedron*, 2020, DOI: 10.1016/j.poly.2020.114884.

70 B. Sen, E. Subasi, H. K. Kalhan, V. Demir, E. E. Güler and H. A. Kayali, Crystal structures, spectroscopic properties of new cobalt(II), nickel(II), zinc(II) and palladium(II) complexes derived from 2-acetyl-5-chloro thiophene thiosemicarbazone: Anticancer evaluation, *Mat. Sci. Engin. C*, 2019, **98**, 550, DOI: 10.1016/j.msec.2018.12.080.

71 T. A. Yousef and G. M. Abu El-Reash, Synthesis, and biological evaluation of complexes based on thiosemicarbazone ligand, *J. Mol. Struct.*, 2020, **1201**, 127180, DOI: 10.1016/j.molstruc.2019.127180.

72 M. M. Fousiamola, M. Sithambaresanb, K. K. Damodaranc and M. R. P. Kurup, Syntheses, spectral aspects and biological studies of bromide and azide bridged box dimer copper(II) complexes of an NNO donor aroylhydrazone, *Inorg. Chim. Acta*, 2020, **501**, 119301, DOI: 10.1016/j.ica.2019.119301.

73 M. Ayad, P. Schollhammer, Y. L. Mest, L. Wojcik, F. Y. Pétillon, N. L. Poul and D. Mandon, Mononuclear copper(II) complexes containing a macrocyclic ditopic ligand: Synthesis, structures and properties, *Inorg. Chim. Acta*, 2019, **497**, 119081, DOI: 10.1016/j.ica.2019.119081.

74 A. A. A. Emara, A. A. Saleh and O. M. I. Adly, Spectroscopic investigations of new binuclear transition metal complexes of Schiff bases derived from 4, 6-diacetylresorcino l and 3-amino-1-propanol or 1, 3-diamino-propane, Spectrochim, *Spectrochim. Acta, Part A*, 2007, **68**, 592, DOI: 10.1016/j.saa.2006.12.034.

75 G. Reshma, V. Padmanabhan, A. R. Varma, M. S. Gouri, U. R. Nai, P. B. Parvathy, N. V. Kulkarni and D. Senthurpandi, Synthesis and structure of mono and bis{1,3-bis(2-pyridylimino)isoindoline}supported 3d transition metal complexes, *J. Mol. Struct.*, 2021, **1226**, 129344, DOI: 10.1016/j.molstruc.2020.129344.

76 N. N. Greenwood, A. Earnshaw, *Chemistry of the Elements*, Pergamon Press, New York, 1984.

77 M. Shebl, S. M. E. Khalil, S. A. Ahmed and H. A. A. Medien, Synthesis, spectroscopic characterization and antimicrobial activity of mono-, bi- and tri-nuclear metal complexes of a new Schiff base ligand, *J. Mol. Struct.*, 2010, **980**, 39–50, DOI: 10.1016/j.molstruc.2010.06.034.

78 O. M. I. Adly, Characterization, molecular modeling and antimicrobial activity of metal complexes of tridentate Schiff base derived from 5-acetyl-4-hydroxy-2H-1,3-thiazine-2,6(3H)-dione, *Spectrochim. Acta, Part A*, 2012, **95**, 483, DOI: 10.1016/j.saa.2012.04.030.

79 J. C. Bailar, H. J. Emeleus, R. Nyholm, A. F. Trotman-Dickenson, *Comprehensive Inorganic Chemistry*, Pergamon Press, 1975, vol. 3.

80 M. Shebl, Synthesis, spectroscopic characterization and antimicrobial activity of binuclear metal complexes of a new asymmetrical Schiff base ligand: DNA binding affinity of copper(II) complexes, *Spectrochim. Acta, Part A*, 2014, **117**, 127, DOI: 10.1016/j.saa.2013.07.107.

81 F. A. Cotton and G. Wilkinson, *Advanced Inorganic Chemistry*, John Wiley and Sons, New York, 4th edn, 1980.

82 M. Mashaly, T. M. Ismail, S. B. El Maraghy and H. A. Habib, Heteronuclear complexes of oxorhenium(V) with Fe(III), Co(II), Ni(II), Cu(II), Cd(II) and UO2(VI) and their biological activities, *J. Coord. Chem.*, 2004, **57**, 1099, DOI: 10.1080/00958970412331281881.

83 M. Shebl, S. M. E. Khalil, M. A. A. Kishk, D. M. EL-Mekkawi and M. Saif, New less toxic zeolite-encapsulated Cu(II) complex nanomaterial for dual applications in biomedical field and wastewater remediation, *Appl. Organomet. Chem.*, 2019, **33**, e5147, DOI: 10.1002/aoc.5147.

84 E. M. Abdelrhman, B. A. El-Shetary, M. Shebl and O. M. I. Adly, Coordinating behavior of hydrazone ligand

bearing chromone moiety towards Cu(II) ions: Synthesis, spectral,density functional theory (DFT) calculations, antitumor, and docking studies, *Appl. Organomet. Chem.*, 2021, **35**, e6183, DOI: 10.1002/aoc.6183.

85 M. Saif, H. F. El-Shafiy, M. M. Mashaly, M. F. Eid, A. I. Nabeel and R. Fouad, Hydrothermal preparation and physicochemical studies of new copper nano-complexes for antitumor application, *J. Mol. Struct.*, 2018, **1155**, 765, DOI: 10.1016/j.molstruc.2017.11.043.

86 M. Saif, H. F. El-Shafiy, M. M. Mashaly, M. F. Eid, A. I. Nabeel and R. Fouad, Synthesis, characterization, and antioxidant/cytotoxic activity of new chromone Schiff base nano-complexes of Zn(II), Cu(II), Ni(II) and Co(II), *J. Mol. Struct.*, 2016, **1118**, 75, DOI: 10.1016/j.molstruc.2016.03.060.

87 C. L. Edelstein and R. W. Schrier, Pathophysiology of ischemic acute renal injury, in *Diseases of the Kidney and Urinary Tract*, R.W. Schrier, Lippincott Williams and Wilkins, Philadelphia, 2007, p. 930.

88 R. Fouad and O. M. I. Adly, Novel Cu(II), Zn(II) Nanocomplexes Drug Based on Hydrazone Ligand Bearings Chromone & Triazine moiety: Structural, Spectral, DFT, Molecular Docking and Cytotoxic Studies, *J. Mol. Struct.*, 2021, **1225**, 129158, DOI: 10.1016/j.molstruc.2020.129158.

89 V. D. Malcic, Z. B. Mikocevic and K. Itric, *KUBELKA-MUNK THEORY IN DESCRIBING OPTICAL PROPERTIES OF PAPER (I) Technical Gazette 18 (2011) 117–24* https://hrcak.srce.hr/file/98650.

90 B. M. Weckhuysen and R. A. Schoonheydt, Recent progress in diffuse reflectance spectroscopy of supported metal oxide catalysts, *Catal. Today*, 1999, **49**, 441, DOI: 10.1016/S0920-5861(98)00458-1.

91 F. Yakuphanoglu, R. Mehrotra, A. Gupta and M. Munoz, Nanofiber organic semiconductors: The effects of nanosize on the electrical charge transport and optical properties of bulk polyanilines, *J. Appl. Polym. Sci.*, 2009, **114**, 794, DOI: 10.1002/app.28535.

92 J. Tauc, *Amorphous and Liquid Semiconductors*: Plenum Press. London and New York, 1974.

93 S. S. Shenouda, M. S. A. Hussien, B. Parditka, A. Csík, V. Takats and Z. Erdélyi, Novel amorphous Al-rich Al_2O_3 ultra-thin films as active photocatalysts for water treatment from some textile dyes, *Ceram. Int.*, 2020, **46**, 7922–7929, DOI: 10.1016/j.ceramint.2019.12.012.

94 K. Abou-Melha, Spectral, modeling and anticancer activity studies on the newly synthesized N-allyl-2-(2,4-dinitrophenyl)hydrazine-1-carbothioamide and some bivalent metal complexes, *J. Mol. Struct.*, 2021, **1223**, 128949, DOI: 10.1016/j.molstruc.2020.128949.

95 N. M. Hosny, M. H. Abdel-Rhman, N. Y. Hassan and H. M. Mahmoud, Spectral, optical and cytotoxicity studies on 2-isonicotinoyl-Nphenylhydrazine-1-carboxamide(H_3L) and some of its metalcomplexes, *J. Mol. Struct.*, 2018, **1156**, 602, DOI: 10.1016/j.molstruc.2017.11.114.

96 S. S. Shenouda, H. Y. Zahran and I. S. Yahia, Facile synthesis and characterization of Co_3O_4 nanoplates coated with small nanorods, *Mater. Res. Express*, 2019, **6**, 105042, DOI: 10.1088/2053-1591/ab3942.

97 N. A. El-Ghamaz, A. Z. El-Sonbati, M. A. Diab, A. A. El-Bindary, G. G. Mohamed and Sh. M. Morgan, Correlation between ionic radii of metal azodye complexes and electrical conductivity, *Spectrochim. Acta, Part A*, 2015, **147**, 200, DOI: 10.1016/j.saa.2015.03.040.

98 M. A. El-ghamry, K. M. Nassir, F. M. Elzawawi, A. A. Abdel Aziz and S. M. Abu-El-Wafa, Novel nanoparticle-size metal complexes derived from acyclovir. Spectroscopic characterization, thermal analysis, antitumor screening, and DNA cleavage, as well as 3D modeling, docking, and electrical conductivity studies, *J. Mol. Struct.*, 2021, **1235**, 130235, DOI: 10.1016/j.molstruc.2021.130235.

99 A. K. Jonscher, The 'universal' dielectric response, *Nature*, 1977, **267**, 673–679.

100 H. Y. Zahran, S. S. Shneouda, I. S. Yahia and F. El-Tantawy, Facile and rapid synthesis of nanoplates $Mg(OH)_2$ and MgO via Microwave technique from metal source: structural, optical and dielectric properties, *J. Sol-Gel Sci. Technol.*, 2018, **86**, 104, DOI: 10.1007/s10971-018-4613-2.

101 I. G. Austin and N. F. Mott, Polarons in crystalline and non-crystalline materials, *Adv. Phys.*, 1969, **18**, 41, DOI: 10.1080/00018736900101267.

102 N. A. Hegab, M. A. Afifi, H. E. Atyia and A. S. Farid, ac conductivity and dielectric properties of amorphous Se80Te20−xGex chalcogenide glass film compositions, *J. Alloy. Comp.*, 2009, **477**, 925, DOI: 10.1016/j.jallcom.2008.11.129.

103 S. R. Elliott, Temperature dependence of a.c. conductivity of chalcogenide glasses, *Phil. Mag. B*, 1978, **37**, 135, DOI: 10.1080/01418637808226448.

104 S. R. Elliot, AC conductivity due to intimate pairs of charged defect centres, *Solid State Comm*, 1978, **27**, 749.

105 M. Fadel, N. A. Hegab, I. S. Yahia, A. M. Salem and A. S. Farid, Electrical and switching properties of Se85Te15−xSbx ($0 \leq x \leq 6$ at.wt%) thin films, *J. Alloys and Compounds*, 2011, **509**, 7663, DOI: 10.1016/j.jallcom.2011.04.093.

106 Nitika and A. Rana, Study of anneal-tuned dielectric properties, AC conductivity, complex impedance, and modulus of cobalt ferrite nanoparticles, *Materials Today: Proceedings*, 2021, **45**, 5444, DOI: 10.1016/j.matpr.2021.02.118.

107 B. Tareev, *Physics of dielectric Materials*, Mir Publishers. Moscow, 1975.

108 A. H. Ahmed and M. G. Moustafa, Spectroscopic, morphology and electrical conductivity studies on Co(II), Ni(II), Cu(II) and Mn(II)-oxaloyldihydrazone complexes, . *Journal of Saudi Chemical Society*, 2020, **24**, 381, DOI: 10.1016/j.jscs.2020.02.003.